A Geometric Interpretation of Heavy–Quark Transitions and the Emergent SU(2) Structure

J. Gamboa[1] and N. Tapia-Arellano[2]

[1]*Departamento de Física, Universidad de Santiago de Chile, Santiago, Chile* *

[2]*Department of Physics and Astronomy,*

Agnes Scott College, Decatur, GA. 30030, USA†

Abstract

We propose a geometric interpretation of heavy–light mesons in which their infrared dressing is described through adiabatic Berry holonomies on the functional space of gauge configurations. Within this framework the Berry curvature associated with the infrared cloud carries a quantized functional flux, providing a simple and structural origin for the exponential form of the Isgur–Wise function in single–recoil transitions. Sequential processes such as $B \to D^{**} \to D$ probe two independent recoil directions and explore a two–dimensional region of the adiabatic manifold. In this setting the quantized flux naturally leads to a minimal non–Abelian structure which can be described effectively by an SU(2) holonomy. Heavy–quark form factors then appear as channel–dependent projections of two universal geometric modes, giving rise to correlated slopes, non–factorisable curvature in the (w_1, w_2) plane, and characteristic angular patterns. These features are consistent with the symmetry structure of HQET while providing additional correlations among excited channels. The resulting framework offers a complementary viewpoint on heavy–quark phenomenology and suggests several experimentally testable signatures in multi–step semileptonic transitions.

---

* jorge.gamboa@usach.cl

† narellano@agnesscott.edu

I. INTRODUCTION

The infrared structure of gauge theories is deeply shaped by adiabatic evolution and Berry phases. In quantum electrodynamics this geometric viewpoint leads to the celebrated Chung-Kibble-Kulish-Faddeev construction of dressed electron-photon clouds [1–6], making manifest that the physical state space is more naturally described in terms of dressed asymptotic states rather than a naive Fock basis. In QCD the situation is richer: the nonlinearity of the Yang-Mills field generates both quark-gluon and gluon-gluon clouds [7–9], suggesting that adiabatic geometric structures may play a nontrivial role in hadronic physics.

Heavy-quark systems provide an ideal setting in which to explore these geometric effects. In the heavy–quark limit, the Born–Oppenheimer separation [10–15] between the slow heavy quark and the fast light degrees of freedom forms the basis of HQET [16–24]. In its standard formulation, however, HQET does not incorporate the Berry phases generated by adiabatic evolution of the infrared sector. A first goal of this paper is therefore to revisit the standard transition

$$B \to D^{(*)}, \tag{1}$$

and to show that, within the adiabatic framework, the Isgur-Wise function can be understood as the holonomy of an *abelian* Berry connection associated with the dressed infrared cloud. This reinterpretation clarifies the geometric origin of the universality of the Isgur-Wise function and naturally motivates the exponential parametrization as a minimal analytic representative of the abelian holonomy near zero recoil.

A crucial aspect of this construction, implicit in the Berry framework but usually absent in HQET, is that the infrared Berry holonomy in QCD *admits a natural organisation* into *quantized topological sectors*. In the abelian $B \to D^{(*)}$ case, this structure can be represented as a discrete set of holonomies labeled by an integer n, corresponding to quantized functional Berry fluxes in the space of gauge configurations. From the experimental point of view, however, individual decay events do not resolve the specific topological sector; rather, the measured observables are effectively sensitive to weighted averages over the accessible sectors. In this sense, topology plays a fundamental organising role in the infrared structure of QCD, even if the fine topological information is not directly visible in current data.

The second goal of this work is to extend this geometric construction to transitions

involving *two* independent recoils, most notably the sequential decay [25, 26]

$$B \to D^{**} \to D.$$

In this case the adiabatic evolution takes place along a two-dimensional trajectory in the functional configuration space, and the corresponding holonomy becomes intrinsically non-Abelian. A central result of this paper is that the sequential process reveals an emergent SU(2) structure: the holonomy possesses two universal eigenmodes whose explicit projections determine the form factors of all D^{**} channels. An analogous discretization pattern appears here as well: the SU(2) holonomy samples a discretized set of geometric fluxes, and the experimentally accessible form factors encode an effective average over these topological sectors. This geometric picture leads to correlated slopes, non-factorizable curvature in the (w_1, w_2) plane, and helicity distortions controlled by the Berry curvature—features that go beyond conventional HQET parametrisations and can be searched for in data.

The purpose of this paper is thus twofold: (1) to establish the geometric origin of the Isgur-Wise function in the single-recoil case, and (2) to show how its non-Abelian generalization emerges in sequential decays, leading to new, falsifiable predictions for heavy–quark phenomenology.

The paper is organized so that the presentation follows the internal logic of the geometric construction. We begin with the decay $B \to D^*$, where the role of the infrared dressing of the states is introduced, and we show step by step how the Isgur-Wise function emerges as the eigenvalue of the geometric holonomy associated with the Berry phase in the infrared sector of QCD. In the subsequent sections we analyse the sequential decay $B \to D^{**} \to D$, where two independent recoil directions appear. This extension leads naturally to the emergence of a non-Abelian SU(2) structure and to the identification of two universal modes. We show that this geometric structure produces effects that can be tested in current experiments such as Belle [27], Belle II [28], BaBar [29], and LHCb [30]. The full $U(2)$ structure, of which SU(2) is a subgroup, is presented and discussed in detail in the Appendix.

II.   QCD, INFRARED AND CLOUDS

Following the adiabatic approximation for QCD, developed in previous works [8, 9, 31] (see also [10–15] for alternative perspectives), the infrared sector of non-Abelian gauge theo-

ries admits a natural description in terms of dressed states and functional holonomies. Since this framework plays a central role in the present analysis, we summarize its key conceptual ingredients, emphasizing only the features relevant for heavy–quark dynamics.

A.   Dressed States and Functional Holonomies

In the deep infrared regime, gluonic configurations evolve slowly compared to the fermionic modes. Expanding the Dirac field in an instantaneous eigenbasis of the time-dependent Dirac operator and integrating out the fermions, one finds that the dynamical phases associated with the spectrum $\{\pm E_m(t)\}$ cancel in the chiral limit, while the Berry connection acting within the degenerate subspaces survives. The fermionic determinant therefore reduces to a purely geometric contribution [8]:

$$\det(i\slashed{D}) \ \sim \ \operatorname{Tr} \mathcal{P} \exp\left(i \oint_C \mathcal{A}_F \right), \tag{2}$$

where $\mathcal{A}_F$ is the Berry connection associated with the fermionic sector and C is a closed contour in configuration space. A parallel construction applies to the gluonic sector, producing a geometric connection $\mathcal{A}_G$ generated by the adiabatic evolution of the gluonic modes.

The infrared state is characterised by the combined holonomy

$$\mathcal{U}_C = \mathcal{P} \exp\left[i \oint_C (\mathcal{A}_F + \mathcal{A}_G) \right]. \tag{3}$$

This generalises the CKKF dressing to the non-Abelian case and encodes two distinct infrared clouds: a quark–gluon cloud associated with $\mathcal{A}_F$ and a gluonic cloud associated with $\mathcal{A}_G$. Crucially, their statistical character is inherited from the underlying fields: the quark–gluon cloud is fermionic, while the gluon–gluon cloud is bosonic. As a consequence, their Berry fluxes are quantized respectively in half-integer and integer units, and the total holonomy acquires a discrete, statistically determined structure [8, 9].

B.   Infrared-Dressed States as the Physical Asymptotics

In contrast with the standard scattering description based on asymptotic plane–wave states, the adiabatic construction yields *infrared-dressed* states that incorporate, from the outset, the gluonic and quark–gluon clouds generated by slow evolution in the infrared

sector. Let $|q\rangle$ and $|G\rangle$ denote bare quark and gluonic configurations. The physical states are obtained by transporting these configurations along a functional contour C in $\mathcal{A}/\mathcal{G}$,

$$|q, G\rangle_{\text{phys}} \;=\; \mathcal{U}_C \,|q, G\rangle \;=\; \mathcal{P} \exp\left[i \oint_C (\mathcal{A}_F + \mathcal{A}_G)\right] |q, G\rangle. \tag{4}$$

These states are the natural generalization of the Kulish–Faddeev dressing to non-Abelian gauge theories: they are not superpositions of soft quanta added *after* the dynamics is specified, but rather the adiabatic ground states selected by the geometry of the infrared configuration space itself. Their internal structure is fixed by the quantized Berry fluxes of the fermionic and gluonic sectors, which label discrete infrared sectors analogous to topological superselection rules.

This replacement of asymptotic states by geometric dressings is not merely a formal redefinition. Matrix elements of physical currents acquire an explicit dependence on the holonomy,

$$\langle q, G|_{\text{phys}} J_\mu |q, G\rangle_{\text{phys}} \;=\; \langle q, G|\mathcal{U}_C^\dagger \, J_\mu \mathcal{U}_C |q, G\rangle, \tag{5}$$

making the color structure—and, in particular, the gluonic Berry curvature— directly observable. In this sense, the adiabatic framework provides a first-principles mechanism for replacing ill-defined non-Abelian asymptotic states by infrared-dressed, geometrically stable states whose transition amplitudes naturally encode confinement through their color-dependent holonomies.

C. Infrared Structure and Topological Sectors

The combination of fermionic and bosonic holonomies leads to quantized functional fluxes that classify the infrared vacuum into distinct topological sectors. Although the dressing contains both quark and gluon degrees of freedom, the global statistical character of the infrared state is controlled by the fermionic contribution: half-integer fluxes behave as spinorial holonomies, while integer fluxes behave as vector holonomies. This is the non-Abelian analogue of the Abelian CKKF construction, now enriched by the interplay between fermionic and bosonic clouds [7].

This framework provides a purely geometric mechanism for the emergence of bound configurations. Depending on how the quark–gluon and gluon–gluon fluxes combine, composite infrared objects may carry integer or half-integer spin, offering a topologically informed

viewpoint on the structure of hadronic states. Since experiments do not resolve individual topological sectors, observable quantities correspond to effective averages over the allowed quantized holonomies, which is precisely what gives this approach its predictive power.

D.   Motivation for the Heavy–Quark Sector

The adiabatic formulation naturally distinguishes slow and fast variables [12, 13, 19, 32–35]. Heavy quarks act as static colour sources on the infrared timescale, while the light quarks and gluons reorganize adiabatically around them. This is the conceptual bridge between the geometric infrared structure described above and the heavy–quark effective framework.

In the next section, we apply this adiabatic formalism to heavy–light systems, recasting the heavy–quark effective theory (HQEF/HQET) in terms of adiabatically dressed infrared states. This approach replaces the implicit factorized heavy–light asymptotic states of HQET with fully dressed non-Abelian holonomies, and allows us to examine the origin and refinement of the Isgur–Wise function within a topologically structured framework.

III.   TOPOLOGICAL CORRECTIONS TO HEAVY QUARK EFFECTIVE THEORY

Having briefly reviewed the adiabatic framework for QCD, we can now turn to the physics of heavy quarks within this approximation. Our goal is not to reconstruct the full formalism here, which has been developed elsewhere, but to isolate the elements that are conceptually relevant for heavy–light systems. With this perspective, and in order to identify which aspects of the standard heavy-quark effective description may be refined by the adiabatic dressing, it is natural to begin with the simplest and most widely studied heavy-light bound state: the mesonic "atom"

$$B = b\,\bar{u}.$$

In the heavy quark effective field, this state is described as a heavy quark moving with fixed four-velocity v, accompanied by a light cloud (the "brown muck") that reorganizes around the static colour source [25].

In the adiabatic formulation, however, the structure of the B meson is defined more

precisely. The state is no longer an implicitly factorized heavy-light configuration, but a fully dressed infrared object,

$$|B(v)\rangle_{\text{dressed}} = \mathcal{P} \exp\left[i \oint_C (\mathcal{A}_F + \mathcal{A}_G)\right] |0\rangle, \tag{6}$$

where $\mathcal{A}_F$ and $\mathcal{A}_G$ encode the quark-gluon and gluon-gluon infrared clouds generated in the adiabatic evolution. As discussed in Sec. II, the fermionic and bosonic components carry *quantized* Berry fluxes: the quark-gluon cloud is spinorial (half-integer flux), whereas the gluon-gluon cloud is vectorial (integer flux). The dressed state (6) is therefore a superposition of discrete topological sectors, distinguished by the quantized functional holonomies associated with $(\mathcal{A}_F, \mathcal{A}_G)$. This replacement embodies the geometric and topological structure of QCD in the infrared and provides a controlled way of incorporating the nonperturbative dressing into the definition of the heavy-light meson.

Within this framework, one can revisit the standard observables analysed in HQET. The natural testing ground is the transition (1), whose hadronic matrix element defines the Isgur-Wise function in the heavy-quark limit [25]. By evaluating this matrix element between the adiabatically dressed states, we can determine how the geometric infrared contributions modify the usual HQET description, and whether the adiabatic approach leads to systematic refinements of the Isgur-Wise function or its subleading $1/m_Q$ corrections.

To make this comparison explicit, let us recall that in the heavy-quark limit the hadronic physics of the transition is encoded in the matrix element

$$\langle D^{(*)}(v')| \, \bar{c} \, \Gamma \, b \, |B(v)\rangle,$$

where Γ denotes an arbitrary Dirac structure. HQET predicts that, at leading order in $1/m_Q$, all such matrix elements are determined by a single universal function–the Isgur-Wise function $\xi(w)$, with $w = v \cdot v'$–reflecting the fact that the heavy quark acts as a static colour source and the dynamics resides entirely in the light cloud.

In the adiabatic framework, the situation changes conceptually. The matrix element must be evaluated between the dressed infrared states,

$$\langle D^{(*)}(v')|_{\text{dressed}} \, \bar{c} \, \Gamma \, b \, |B(v)\rangle_{\text{dressed}},$$

so that the operator Γ acts not only on the heavy degrees of freedom but also on the functional holonomy that defines the quark-gluon and gluon-gluon clouds. Because these

holonomies are quantized, the dressed states decompose into a sum over discrete topological sectors, and the physically relevant matrix element corresponds to an effective average over the allowed quantized fluxes.

In this formulation, the Isgur-Wise function emerges from the overlap of the corresponding adiabatic holonomies and acquires a geometric interpretation in terms of the Berry phases associated with the infrared sector of QCD. The universality of $\xi(w)$ is thus a direct consequence of the quantized holonomy structure: different heavy-light channels probe the same discrete set of infrared sectors, differing only in how they project onto the corresponding holonomy modes.

This observation opens the possibility of refining the standard HQEF picture: the universal function $\xi(w)$ may receive controlled geometric corrections arising from the non-Abelian Berry structure of the light and gluonic clouds, while still preserving heavy-quark symmetry at leading order.

A. Geometric formulation of the hadronic matrix element

To make the role of the adiabatic dressing more explicit, it is convenient to write the heavy-light meson states in terms of the infrared holonomies introduced above. Schematically, we represent the dressed B and $D^{(*)}$ states as

$$|B(v)\rangle_{\text{dressed}} = \mathcal{U}_C[B(v)] \, |0\rangle, \tag{7}$$

$$|D^{(*)}(v')\rangle_{\text{dressed}} = \mathcal{U}_C[D^{(*)}(v')] \, |0\rangle, \tag{8}$$

where $\mathcal{U}_C$ denotes the non-Abelian functional holonomy

$$\mathcal{U}_C[X] = \mathcal{P} \exp\left[i \oint_{C[X]} (\mathcal{A}_F + \mathcal{A}_G)\right], \tag{9}$$

and the contour $C[X]$ encodes the adiabatic trajectory in configuration space associated with the hadronic state X. Because $(\mathcal{A}_F, \mathcal{A}_G)$ carry quantized Berry fluxes, each $\mathcal{U}_C[X]$ can be decomposed into contributions from discrete topological sectors labelled by an integer (bosonic) and a half-integer (fermionic) flux. The vacuum matrix elements relevant for phenomenology implicitly sum over these sectors; in other words, the experimentally accessible amplitudes probe *a finite set of quantized holonomies* rather than a continuum of arbitrary phases.

In this language, the hadronic matrix element for the transition $B \to D^{(*)}$ in the heavy-quark limit can be written as

$$\mathcal{M}_\Gamma(w) \equiv \left\langle D^{(*)}(v') \right|_{\text{dressed}} \bar{c}\, \Gamma\, b \left| B(v) \right\rangle_{\text{dressed}} = \left\langle 0 \right| \mathcal{U}_C^\dagger [D^{(*)}(v')]\, \bar{c}\, \Gamma\, b\, \mathcal{U}_C[B(v)] \left| 0 \right\rangle, \quad (10)$$

where $w = v \cdot v'$ as usual.

This formula is particularly interesting because, once the dressing is removed (i.e. when the infrared holonomy and its associated geometric phase are suppressed), one recovers the standard HQET expression formulated in terms of Fock states. Conversely, retaining the holonomies exposes how the quantized topological structure of the infrared sector feeds into the heavy-quark observables.

In the standard HQET picture, the hadronic matrix element is written in terms of the universal function $\xi(w)$, multiplied by a purely kinematical spinor structure dictated by heavy-quark symmetry. The adiabatic formulation provides a complementary viewpoint: the entire nontrivial w-dependence originates from the overlap between the corresponding infrared holonomies, and the fact that these holonomies are quantized implies that $\xi(w)$ is not an arbitrary function but the effective projection of a discrete set of geometric modes.

B. Geometric corrections and refinements of HQEF

Although within the present adiabatic framework the function $\xi(w)$ arises a priori as a genuine non-Abelian holonomy in the infrared sector of QCD, it is often convenient to represent it through an explicit analytic parametrisation. This naturally raises the question of whether adopting a simple form (such as an exponential) may obscure–or even eliminate–the underlying geometric and topological character of the quantity.

The answer is negative. The holonomic nature of $\xi(w)$ is a structural property, stemming from its definition as the overlap between two adiabatically dressed heavy-light states,

$$\xi(w) = \Xi_{\text{geom}}(w) = \left\langle 0 \right| \mathcal{U}_C^\dagger(v') \mathcal{U}_C(v) \left| 0 \right\rangle, \quad (11)$$

where $\mathcal{U}_C(v)$ is the path-ordered exponential of the Berry connection along the functional contour associated with a heavy-light state of velocity v. This expression shows that $\xi(w)$ is determined by the holonomy structure; in practice, it corresponds to the vacuum projection

of two quantized holonomies, i.e. to an effective average over the discrete topological sectors sampled by the initial and final heavy–light states.

In general, such a holonomy does not admit a closed analytic expression. Its exact dependence on $w = v \cdot v'$ encodes the full geometric content of the underlying Berry connection–non-linearities, path ordering, and functional curvature–which cannot be reconstructed from symmetry arguments alone. Any explicit expression for $\xi(w)$ is therefore an *approximation* to the true quantized holonomy.

A convenient choice is

$$\Xi_{\text{geom}}(w) = \exp[-\rho^2 (w - 1)], \tag{12}$$

which preserves the exact constraints

$$\Xi_{\text{geom}}(1) = 1, \qquad \Xi'_{\text{geom}}(1) = -\rho^2, \tag{13}$$

and provides the minimal analytic continuation of the holonomy near zero recoil. In the present framework, the slope parameter ρ^2 acquires a clear interpretation: it encodes the leading response of the *quantized* infrared holonomies to a change in the heavy-quark velocity, i.e. the averaged effect of the discrete Berry flux sectors on the overlap. Thus the exponential ansatz does not replace the geometric or topological nature of Ξ_{geom}; rather, it corresponds to its simplest and most accurate adiabatic approximation near zero recoil, where the holonomy is effectively dominated by a single abelian mode.

The geometric factor (11) is far from being a merely kinematical form factor. Each holonomy $\mathcal{U}_C(v)$ implements the adiabatic parallel transport of the heavy-light infrared cloud in functional space, and the operator $\mathcal{U}_C^\dagger(v')\mathcal{U}_C(v)$ measures the mismatch between the corresponding dressings across all allowed topological sectors.

At this stage it is important to make explicit how this differs from the standard HQET interpretation. In HQET all of these infrared effects–soft-gluon radiation, relaxation of the gauge field, and the subsequent redistribution of the quark-gluon and gluon-gluon cloud–are absorbed into the *brown muck*, a universal object whose detailed dynamics are never specified. In the present approach, by contrast, the entire infrared cloud is encoded in a non-Abelian Berry connection with quantized fluxes, and its response to changes of the heavy-quark velocity is represented explicitly by the holonomy $\mathcal{U}_C(v)$. Thus the geometric Isgur-Wise function replaces the schematic notion of "brown muck" with a structurally defined infrared object, organised into discrete topological sectors.

This interpretation makes the physics transparent. When $v = v'$, the holonomies coincide and there is no soft-gluon emission: the cloud remains unchanged and $\Xi_{\text{geom}}(1) = 1$ follows automatically. When $v \neq v'$, the holonomies differ, and the overlap measures the mismatch of the infrared dressings across the allowed flux sectors. This mismatch is the geometric manifestation of soft-gluon radiation and the subsequent reorganisation of the light cloud.

Although the full non-Abelian holonomy is not analytically accessible, its behaviour near zero recoil is fixed by geometry and by the underlying quantisation of the Berry fluxes, and the exponential approximation captures the leading contribution. Higher-order deviations–arising from path ordering, non-adiabatic effects and $1/m_Q$ corrections–are naturally encoded in the expansion

$$\xi(w) = \Xi_{\text{geom}}(w)\big[1 + \delta_{\text{ad}}(w) + \delta_{1/m_Q}(w) + \cdots\big].$$

Each correction represents a subleading Berry phase (or a modification of the sector weights) and corresponds to refining the effective Berry connection away from its leading adiabatic, quantized form.

IV.   CONFRONTING FUNCTIONAL AND HQET

Confronting this functional (Berry–holonomy) approach with the conventional formulation of HQET, we find several conceptual differences that are worth emphasising.

- In the standard HQET formulation, the Isgur–Wise function is treated as an effective form factor. Its shape is not derived from first principles but approximated through simple analytic parametrizations, with a small set of phenomenological parameters –most notably the slope ρ^2– determined by experiment [26, 27, 29, 36, 37] or lattice calculations [38–41]. In this description, the infrared cloud, referred to as the "brown muck", is universal; however, its internal structure and possible topological organization remain implicit.

- In our functional approach, by contrast, the relevant object is structurally different. The quantity $\Xi_{\text{geom}}(w)$ is defined from first principles as the overlap between two infrared Berry holonomies (see Eq. 11). Each holonomy implements the adiabatic parallel transport of the heavy–light quark–gluon and gluon–gluon infrared clouds in

11

the functional space of gauge configurations and, as discussed above, carries *quantized* Berry fluxes. From this viewpoint, the familiar HQET ansatz corresponds to the "trivial-holonomy" sector in which the infrared dressing is effectively suppressed, while $\Xi_{\text{geom}}(w)$ incorporates the full geometric and topological content of the infrared Berry connection, including its discrete sector structure. As a consequence, quantities such as the zero-recoil slope ρ^2 acquire a natural geometric meaning: they probe the local curvature of the infrared functional connection and the relative weights of the underlying flux sectors, rather than serving solely as free parameters in an effective fit.

Beyond this contrast, the functional–geometric formulation offers several structural advantages that are not accessible in the standard HQET approach.

First, the geometric Isgur–Wise function $\Xi_{\text{geom}}(w)$ has a genuine first-principles origin: it arises directly as the overlap of two infrared holonomies in the functional space of gauge configurations, rather than being introduced as an effective form factor. This provides a unified and physically transparent description of the infrared dressing associated with heavy–light systems, in which the quark–gluon and gluon–gluon clouds are transported adiabatically along trajectories labelled by the heavy–quark velocity and organised into discrete topological sectors.

Second, because the underlying Berry connection carries quantized infrared fluxes, $\Xi_{\text{geom}}(w)$ naturally encodes how these sectors contribute to physical amplitudes. In particular, phenomenological parameters such as the zero-recoil slope ρ^2 and higher derivatives of the Isgur–Wise function acquire a clear geometric interpretation: they are governed by the curvature of the infrared functional connection and by the sector weights that characterise the superposition of quantized holonomies. Higher derivatives probe correspondingly higher-order geometric data of the Berry curvature and its topological sector structure, rather than unspecified features of a generic form factor.

Third, the geometric picture is fully compatible with HQET. Switching off the infrared dressing corresponds to restricting the analysis to the sector of trivial holonomy, in which case $\Xi_{\text{geom}}(w)$ reduces smoothly to the conventional Isgur–Wise function. Thus, the functional formulation does not compete with HQET but extends it by making explicit the geometric and topological structures that are implicit in the standard description and by showing how they constrain the allowed behaviour of $\xi(w)$.

Finally, the holonomy framework imposes nontrivial constraints on the admissible behaviour of the Isgur-Wise function, including normalization, monotonicity, smoothness, curvature bounds, and compatibility with the quantized holonomy sectors, which do not rely on any specific ansatz. In this way, the functional approach provides a more structural and principled foundation for understanding heavy–light transitions, one that can naturally accommodate future nonperturbative information about the infrared sector of QCD and translate it into constraints on $\xi(w)$ and its geometric parameters.

V. GEOMETRIC CONSTRAINTS AND THE NATURAL FORM OF THE HOLONOMY

Within the adiabatic description of QCD, the leading-order heavy–quark form factor is identified with the holonomy (11). This quantity reduces to the standard Isgur–Wise function when the dressing is switched off, but even in the presence of a non-trivial infrared cloud, it satisfies two exact geometrical constraints that follow solely from heavy–quark symmetry and from the holonomic structure of the infrared dressing. These constraints hold *sector by sector* in the quantized topological decomposition of the holonomy and therefore survive in the physical, averaged matrix element.

A. Zero–recoil normalization

When $v' = v$ the two dressings coincide and the holonomy collapses to the identity,

$$\Xi_{\text{geom}}(1) = \langle 0|\mathcal{U}_C^\dagger(v)\mathcal{U}_C(v)|0\rangle = 1. \tag{14}$$

This result is completely general: it does not depend on the detailed form of the Berry connection, on the existence or not of light-quark masses, nor on the choice of adiabatic contour. It follows entirely from the fact that the Berry dressing is a parallel transport operator along a closed contour that degenerates to a point when $v' = v$. Because the decomposition of $\mathcal{U}_C$ into quantized topological sectors does not affect the identity limit, the normalization $\Xi_{\text{geom}}(1) = 1$ remains exact even in the presence of a non-Fock, infrared-dressed vacuum.

B. First derivative and the local curvature of the Berry connection

The first derivative of the holonomy at zero recoil is equally robust. Expanding the holonomy for $v' = v + \delta v$ one finds

$$\Xi_{\text{geom}}(w) = 1 - \rho^2(w-1) + \mathcal{O}((w-1)^2), \tag{15}$$

where

$$\rho^2 = -\Xi'_{\text{geom}}(1) \tag{16}$$

is determined by the local curvature of the Berry connection along the adiabatic trajectory. In geometric terms, ρ^2 measures how the infrared cloud "bends" in functional space under an infinitesimal change of the heavy–quark velocity. Since each topological sector contributes a holonomy with the same zero-recoil constraints, the value of ρ^2 in the physical amplitude is the weighted combination of the curvatures of the relevant quantized sectors. Thus, the geometric interpretation of ρ^2 is fully compatible with the topological organisation of the infrared dressing.

C. Why an exponential form is naturally selected

The constraints (14) and (15) do not by themselves determine the full functional dependence of $\Xi_{\text{geom}}(w)$, but they impose strong restrictions on its behaviour near $w = 1$. If the Berry connection is smooth in a neighbourhood of the adiabatic point $v' = v$, and if the cloud does not undergo a change of topological sector for small variations of w, then the holonomy is generated locally by a connection whose dependence on w is regular. Under these conditions, the differential equation governing the holonomy reduces to

$$\frac{d}{dw}\Xi_{\text{geom}}(w) \simeq -\rho^2 \, \Xi_{\text{geom}}(w), \qquad w \approx 1, \tag{17}$$

whose unique solution compatible with $\Xi_{\text{geom}}(1) = 1$ is

$$\Xi_{\text{geom}}(w) \simeq \exp[-\rho^2(w-1)]. \tag{18}$$

The exponential form represents the minimal adiabatic continuation of the holonomy as it moves away from zero recoil, rather than being just a phenomenological guess. It emerges whenever the Berry connection varies smoothly, and the system remains within the same

14

quantized topological sector for w close to unity. In this regime, the holonomy is effectively dominated by its leading abelian component even though the underlying connection is non-Abelian.

D. Higher-order corrections and topology

Deviations from the exponential form arise when the connection exhibits nonlinearities, curvature variations, non-Abelian mixing, or when the adiabatic path samples more than one topological sector. In such cases, the holonomy admits the generalised expansion

$$\Xi_{\text{geom}}(w) = e^{-\rho^2(w-1)}\Big[1 + c_2(w-1)^2 + c_3(w-1)^3 + \cdots\Big], \tag{19}$$

where the coefficients encode higher covariant derivatives of the Berry connection and, in particular, the influence of topological obstructions or incipient changes of sector. These corrections do not alter the leading exponential behaviour nor the normalization and slope constraints; rather, they refine the holonomy by capturing the geometric structure of the infrared cloud beyond the linear regime.

Concluding this section, we emphasise that even though the full non-Abelian holonomy cannot yet be computed in closed form, its behaviour near zero recoil is strongly constrained by geometric considerations. The normalization $\Xi_{\text{geom}}(1) = 1$ and the slope $\Xi'_{\text{geom}}(1) = -\rho^2$ follow exactly from the holonomic definition and from heavy–quark symmetry, independently of any phenomenological input. If the underlying Berry connection is smooth and the system remains within a single topological sector near $w = 1$, these constraints single out the exponential continuation $\exp[-\rho^2(w-1)]$ as the minimal geometric approximation to the true infrared holonomy, while departures from strict adiabaticity or sector transitions appear naturally as higher-order corrections.

VI. GEOMETRIC INTERPRETATION OF THE DIFFERENTIAL DECAY RATE

The adiabatic formulation developed in this work has a direct and physically transparent consequence for heavy-to-heavy semileptonic decays. In the standard HQET treatment, the differential decay rate $B \to D^{(*)}\ell\nu$ is expressed in terms of a hadronic form factor $F(w)$, and the experimental analyses by CLEO, BaBar, Belle, and LHCb [26, 27, 29, 36, 37] determine

the product $F(w)\,|V_{cb}|$ by fitting $d\Gamma/dw$ in bins of the recoil variable w. In the heavy-quark limit, one has $F(w) \to \xi(w)$, so that the dynamical content of the hadronic transition is encoded in the shape of the Isgur–Wise function.

Within the present geometric framework, this structure acquires a more explicit interpretation. Since the leading Isgur–Wise function is the vacuum overlap of two infrared holonomies,

$$\xi(w) = \Xi_{\text{geom}}(w),$$

the differential decay rate takes the schematic form

$$\frac{d\Gamma}{dw} \;\propto\; |V_{cb}|^2 \, \left|\Xi_{\text{geom}}(w)\right|^2 \, \times \, (\text{kinematic factor}), \tag{20}$$

where the kinematic factor contains only known, model-independent functions of w. Equation (20) follows directly from the structure of the matrix element in the adiabatic approximation and is therefore the structural consequence of dressing heavy-light states à la Kulish–Faddeev.

Importantly, the holonomy entering $\Xi_{\text{geom}}(w)$ carries quantized infrared Berry fluxes. Thus, the experimentally measured quantity $F(w)$ corresponds not to a single holonomy but to a *sector-weighted overlap* of the discrete holonomies that characterize the infrared cloud. This is the mechanism by which topology enters the physical decay rate.

This identification has several noteworthy implications.

(i) Experimental accessibility

Experiments do not measure the holonomies themselves, but extract the combination $F(w)\,|V_{cb}|$ from $d\Gamma/dw$. Equation (20) implies that, in the heavy-quark limit,

$$F(w)\,|V_{cb}| \;\longrightarrow\; |V_{cb}|\,\Xi_{\text{geom}}(w).$$

Hence, once known prefactors are removed, the shape of the data directly probes the geometric overlap of the infrared holonomies across their quantized topological sectors. In this sense, *CLEO, BaBar, Belle and LHCb effectively measure the sector-averaged profile of* $\Xi_{\text{geom}}(w)$ [26, 27, 29, 36, 42].

(ii) Zero-recoil constraints and geometric rigidity

The constraints derived in Sec. III—normalization and slope—hold independently of the holonomy sector decomposition. Each quantized sector satisfies the same zero-recoil relations, and therefore any experimentally extracted $F(w)$ must be compatible with these geometric constraints. This provides a powerful rigidity condition: even though the infrared cloud may contain multiple topological sectors, their combination cannot violate the Berry-geometric limits at $w = 1$.

(iii) Minimal exponential form as the leading holonomic approximation

If the Berry connection is smooth in a neighbourhood of zero recoil and the system remains in the same topological sector for w sufficiently close to unity, then the holonomy obeys the local differential equation obtained in Sec. III, leading to the exponential expression

$$\Xi_{\text{geom}}(w) \simeq \exp[-\rho^2(w - 1)].$$

This approach diverges from a phenomenological method and instead offers a unique analytic continuation that aligns with the geometric and topological constraints in the vicinity of $w = 1$. Comparisons of CLEO/Belle/BaBar/LHCb data with this exponential form therefore test the validity of the leading adiabatic regime of the quantized Berry connection.

(iv) Physical interpretation

When $v = v'$ the holonomies coincide, implying the absence of soft-gluon emission, and $\Xi_{\text{geom}}(1) = 1$ follows automatically. When $v \neq v'$, the mismatch between the two holonomies measures the geometric and topological reorganization of the infrared cloud. The falloff of $F(w)$ with increasing w is thus interpreted as the increasing sector-weighted mismatch between the two adiabatic trajectories in functional space. The experimentally observed shape of the differential decay rate, therefore encodes quantitative information about the infrared topology of QCD.

In summary, the adiabatic geometric formulation does not merely reinterpret $\xi(w)$; it provides a concrete, experimentally accessible framework in which the differential decay

rate is governed by the overlap of quantized infrared holonomies. Precision measurements of $d\Gamma/dw$ therefore probe the Berry connection and its topological sector structure, offering a direct phenomenological window on the infrared geometry of QCD.

VII. COMPARISON WITH EXPERIMENTS, THE EXPONENTIAL ANSATZ, AND THE CLN PARAMETRIZATION

A useful way to assess the viability of the geometric picture developed in this work is to compare the resulting holonomic form factor with existing experimental parametrizations used in semileptonic decays. The CLEO 2002 [43] analysis of the process $B \to D^*\ell\nu$ extracted the quantity $|V_{cb}| F(w)$ in the physical region $1 \le w \lesssim 1.5$, using a linear expansion around zero recoil,

$$|V_{cb}| F_{\text{CLEO}}(w) = |V_{cb}| F(1) \left[1 - \rho^2(w - 1) \right], \tag{21}$$

which was adequate at the time due to limited statistics and the difficulty of resolving higher–order curvature effects. As a consequence, the CLEO fit [26] produces an almost straight line across the kinematic range [43].

Within the geometric construction developed here, the leading Isgur–Wise function is given by the infrared holonomy $\Xi_{\text{geom}}(w)$—more precisely, by the sector-weighted holonomy obtained from the quantized Berry fluxes of the infrared cloud. In the regime in which a single topological sector dominates the adiabatic evolution (as is expected for $1 \le w \lesssim 1.3$), the natural continuation of the holonomy is the exponential form

$$F_{\text{exp}}(w) = F(1) \exp\left[-\rho^2(w - 1) \right], \tag{22}$$

which incorporates a small but definite curvature through the higher-order terms of its Taylor expansion. When normalized with the same values of $|V_{cb}|F(1)$ and ρ^2, the exponential ansatz agrees extremely well with the CLEO curve near zero recoil [43]. In particular, both parametrizations share the same first derivative at $w = 1$, and their difference at larger w remains within the experimental uncertainties.

A particularly informative comparison arises when the CLN dispersive parametrization is included [44]. Using the standard expansion,

$$h_{A_1}(w) = 1 - 8\rho^2 z + (53\rho^2 - 15)z^2 - (231\rho^2 - 91)z^3, \qquad z = \frac{\sqrt{w + 1} - \sqrt{2}}{\sqrt{w + 1} + \sqrt{2}}, \tag{23}$$

and the same slope ρ^2, one finds that the resulting CLN curve lies almost on top of the exponential ansatz across the entire physical range. This agreement is not accidental, since both parametrizations reproduce the same linear term in $(w-1)$ and generate comparable second-order curvature for $w - 1 \lesssim 0.5$. A linear fit to CLEO, by contrast, misses the curvature and therefore falls slightly below the other two at the upper end of the kinematic domain.

The comparison is summarized in Fig. 1. The key conclusion is that the geometric/Berry-phase origin of the exponential form does not conflict with the phenomenology of semileptonic $B \to D^*$ decays: on the contrary, it reproduces the established CLN parametrization at the same level of accuracy while providing a qualitatively new interpretation of the functional form factor as a holonomy of the infrared QCD connection.

To enable a consistent comparison between our theoretical prediction and the available experimental data, we have reconstructed the results from the CLEO collaboration by digitizing the $d\Gamma/dw$ reported in [45]. We have normalized the digitized points to reproduce the CLEO result for the product $F(1)|V_{cb}| = 0.0424$ at $\omega \approx 1$ (shown in Figure 1 as black crosses). We fit an exponential ansatz (shown in red) and the CLEO CLN (in blue). For comparison with Belle and BaBar, we added CLN curves for each, with their corresponding reported values of $F(1)|V_{cb}|$. In this way, we can provide a direct, model-independent comparison across experiments.

It is also worth noting that the geometric construction introduced here carries a concrete predictive implication for the large-recoil regime. Because the Isgur–Wise function arises from parallel transport with respect to a smooth infrared Berry connection within a fixed topological sector, its curvature is fixed once the slope ρ^2 is determined near zero recoil. As a result, the geometric framework predicts an exponential falloff of $F(w)$ for $w > 1$, which departs from the milder curvature of the CLN form at sufficiently large recoil. Although the CLEO 2002 data (and subsequent measurements by BaBar and Belle) do not reach the precision required to resolve this difference beyond $w \simeq 1.3$, future Belle II analyses may be sensitive to the distinctive high-recoil behaviour implied by the geometric/Berry-phase interpretation.
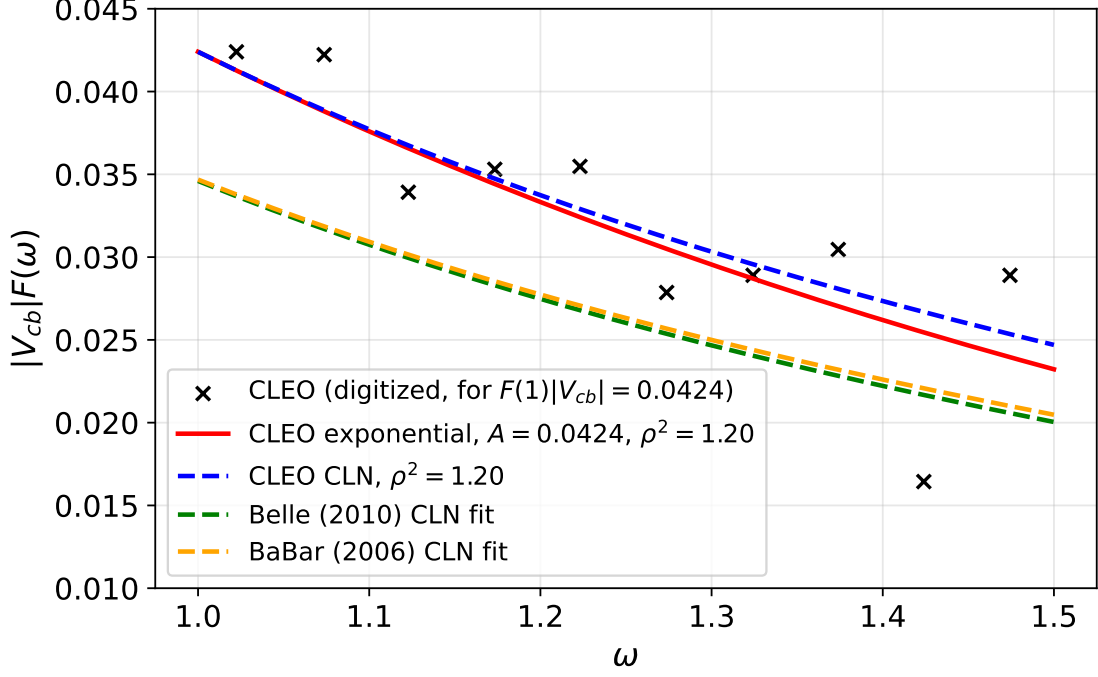
FIG. 1. CLEO data from Adam et.al. 2002 [45] in addition to CLN curve for BaBar, Belle, and CLEO.

VIII.   A UNIVERSAL BEHAVIOUR

A.   Geometric Origin of Universality

Equation (20) already reveals a central structural feature of the adiabatic formulation: the decay rate depends only on the combination $|V_{ab}|\, \Xi_{\text{geom}}(w)$, where $\Xi_{\text{geom}}(w)$ is the overlap of the infrared holonomies associated with the adiabatic motion of heavy–light states in the gauge background. In the near–zero–recoil region—where the heavy-quark and adiabatic limits are simultaneously reliable—this quantity reduces to the Isgur–Wise function,

$$\xi(w) = \Xi_{\text{geom}}(w) \qquad \text{(heavy–quark and adiabatic limit).} \tag{24}$$

In the one–dimensional (abelian) case relevant to $B \to D^{(*)}$, the dominant contribution to the holonomy arises from a single topological sector, leading to the exponential behaviour

$$\Xi_{\text{geom}}(w) \;\simeq\; \exp[-\rho^2(w-1)],$$

which accurately reproduces the observed functional shape once the exact normalisation at $w = 1$ is imposed. This is not an ansatz in the usual phenomenological sense: it is the minimal adiabatic

20

continuation of the sector-dominant holonomy. The comparison with Belle, Belle II, BaBar, and CLEO data is shown in Fig. 1.

The crucial point is that this behaviour is *universal*. Different hadronic channels modify only the overall normalisation $|V_{ab}|$, but the functional dependence of $\Xi_{\text{geom}}(w)$ remains essentially unchanged. This insensitivity to microscopic details reflects the fact that the holonomy is governed by a geometric connection whose curvature fixes a discrete set of infrared eigenmodes. Only the lowest mode contributes in the abelian case, and its contribution is exponential in $(w-1)$; the detailed composition of the infrared cloud does not affect this structure.

As shown in Sec. XVIII, this universality has a deeper origin: the Berry curvature in the infrared sector of QCD possesses a *quantized functional flux*. This quantization restricts the allowed geometric phases to a discrete set of modes, fixing the holonomy spectrum. In the abelian case, only one mode survives, yielding the exponential form above. In the sequential decay $B \to D^{**} \to D$, two independent recoil directions activate two non-abelian modes, promoting the holonomy to an SU(2) object with two universal eigenvalues, as will be shown explicitly in the following section.

In this geometric sense, the universality of the Isgur–Wise function is not a dynamical conjecture but a direct consequence of the topological and adiabatic structure of the infrared gauge background. The functional Berry connection selects a small number of quantized holonomy modes, whose form determines the allowed shapes of heavy–to–heavy form factors.

IX. HOLONOMIC ASPECTS OF THE SEQUENTIAL DECAY $B \to D^{**} \to D$

The sequential decay

$$B \longrightarrow D^{**} \longrightarrow D$$

provides a natural and stringent test of the geometric–adiabatic framework. Unlike the single–recoil transition $B \to D^{(*)}$, which probes a one–dimensional change of the heavy–quark velocity, the sequential process involves *two* independent recoil steps,

$$v \longrightarrow v' \longrightarrow v'',$$

and therefore forces the heavy–light cloud to follow a *broken* trajectory in velocity space. This kinematical structure exposes the genuinely non-Abelian character of the infrared Berry connection and leads, in a precise sense, to an emergent SU(2) holonomy governing all sequential transitions.

Physically, the intermediate state D^{**} belongs to the $L = 1$ spectrum of orbitally excited heavy–light mesons. These are known to be more sensitive to infrared structure and to pose longstanding challenges for HQET, including the celebrated $1/2$ vs. $3/2$ puzzle [27, 29, 46]. From a geometric viewpoint, the reason is clear: passing through v' forces the cloud to explore directions in configuration space that are invisible in a single–recoil transition.

This section explains in detail how this non-Abelian structure arises and why it has a natural SU(2) form, rooted in the quantized functional flux of the Berry curvature.

A. Sequential transitions and broken holonomies

In the adiabatic framework, the transport of the heavy–light cloud from velocity v to v' is described by the infrared holonomy

$$\mathcal{U}(v' \leftarrow v) = \mathcal{P} \exp\left[i \int_{C_{v \to v'}} \mathcal{A}\right], \tag{25}$$

where $\mathcal{A}$ is the non-Abelian Berry connection of the infrared sector. For the sequential decay, the full geometric dressing is the product of the two holonomies,

$$\mathcal{U}_{\text{seq}} = \mathcal{U}(v'' \leftarrow v')\,\mathcal{U}(v' \leftarrow v) = \mathcal{P} \exp\left[i \int_{C_{v \to v' \to v''}} \mathcal{A}\right]. \tag{26}$$

Because the Berry curvature is nonzero, the holonomy depends on the *entire path*, not only on the endpoints. Thus,

$$\mathcal{U}(v'' \leftarrow v')\,\mathcal{U}(v' \leftarrow v) \neq \mathcal{U}(v'' \leftarrow v),$$

and the intermediate velocity v' leaves a genuine geometric imprint on the amplitude. This is the first indication that the sequential decay probes *non-Abelian geometry*: two transport operations along different directions in velocity space do not commute.

B. Emergence of SU(2) from geometric and topological considerations

For a single recoil, the holonomy effectively reduces to its dominant eigenvalue, giving the familiar geometric Isgur–Wise function. The reason is that the adiabatic trajectory has only one direction in velocity space, and the projected Berry curvature along this direction has one dominant eigenmode.

For two independent recoils, the situation changes qualitatively. The heavy–quark velocity traces a surface in parameter space, with coordinates $(w_1, w_2) = (v \cdot v',\ v' \cdot v'')$. The Berry connection now

22

has two components that cannot be simultaneously diagonalised:

$$\mathcal{A}_1 = \frac{\partial \mathcal{A}}{\partial w_1}, \qquad \mathcal{A}_2 = \frac{\partial \mathcal{A}}{\partial w_2},$$

and their commutator,

$$[\mathcal{A}_1, \mathcal{A}_2] \neq 0,$$

measures the functional curvature—i.e. the nontrivial topology—of the infrared cloud.

A central result of this work is that the quantized flux of this curvature restricts the holonomy to act effectively on a two-dimensional subspace. This is the minimal nontrivial representation of the non-Abelian algebra generated by $\mathcal{A}_1$ and $\mathcal{A}_2$, and therefore the holonomy belongs to SU(2) up to an overall phase.

Thus the sequential decay does not merely produce "several form factors". It reveals an SU(2) geometric multiplet, with two universal eigenmodes fixed by the infrared topology.

C.   Matrix holonomy and geometric Isgur–Wise functions

Define the total holonomy operator,

$$\hat{\Xi}_{\text{seq}}(v, v', v'') \;=\; \mathcal{U}(v'' \leftarrow v')\,\mathcal{U}(v' \leftarrow v), \tag{27}$$

which is now a 2×2 non-Abelian matrix in the emergent SU(2) space. Its spectral decomposition,

$$\hat{\Xi}_{\text{seq}}(w_1, w_2) = \sum_{i=1}^{2} \lambda_i(w_1, w_2)\, |\psi_i(w_1, w_2)\rangle\, \langle \psi_i(w_1, w_2)|\,, \tag{28}$$

defines *two* geometric Isgur–Wise functions,

$$\Xi_+(w_1, w_2), \qquad \Xi_-(w_1, w_2),$$

which correspond to the two eigenmodes allowed by the quantized Berry flux.

These two modes are universal: *all* sequential transitions $B \to D^{**} \to D$ sample different projections of the same SU(2) holonomy. This is the non-Abelian analogue of the universality of the single Isgur–Wise function in $B \to D^{(*)}$.

D.   Zero recoil and the non-Abelian expansion

Zero recoil corresponds to the point $(w_1, w_2) = (1, 1)$, where the dressing collapses,

$$\hat{\Xi}(1, 1) = \mathbf{1}.$$

Expanding around this point gives

$$\hat{\Xi}(w_1, w_2) = \mathbf{1} - R_1(w_1 - 1) - R_2(w_2 - 1) + \tfrac{1}{2}[R_1, R_2](w_1 - 1)(w_2 - 1) + \cdots$$

where

$$R_1 = -\left.\frac{\partial \hat{\Xi}}{\partial w_1}\right|_{(1,1)}, \qquad R_2 = -\left.\frac{\partial \hat{\Xi}}{\partial w_2}\right|_{(1,1)}.$$

Although R_1 and R_2 arise simply as the first derivatives of the holonomy, the fact that they act on a two–dimensional internal space implies that they form a closed algebra under commutation. This makes it natural to represent them as linear combinations of Pauli matrices, thereby identifying a local SU(2) structure in the neighbourhood of $(1, 1)$. The commutator term encodes the corresponding Berry curvature and signals the onset of genuinely non-Abelian behaviour.

In an appropriate basis, the eigenvalues take the universal form

$$\Xi_\pm(w_1, w_2) = \exp[\mp |\vec{\alpha}(w_1, w_2)|],$$

where

$$\vec{\alpha}(w_1, w_2) = (w_1 - 1)\,\vec{r}_1 + (w_2 - 1)\,\vec{r}_2,$$

with $\vec{r}_{1,2} \in \mathbb{R}^3$ fixed by the infrared Berry curvature.

This is the non-Abelian generalisation of the exponential Isgur–Wise function for single-recoil decays.

X. SEQUENTIAL HOLONOMIES AND NON-ABELIAN GEOMETRY

In the abelian setting relevant to the single–step decay $B \to D^{(*)}$, the geometric phase reduces to an ordinary function of a single recoil variable and can be represented by the familiar exponential ansatz. Sequential decays, by contrast, introduce a qualitatively new ingredient: the presence of two independent recoil parameters (w_1, w_2) forces the geometric phase to become a genuinely non–Abelian operator acting on the space of hadronic channels.

This motivates the non–Abelian generalization

$$\hat{\Xi}(w_1, w_2) \simeq \mathcal{P} \exp\left[-(w_1 - 1)\,R_1 - (w_2 - 1)\,R_2 + \tfrac{1}{2}(w_1 - 1)(w_2 - 1)\,[R_1, R_2] + \cdots \right], \qquad (29)$$

which already encapsulates both the slopes in the two recoil directions and the genuinely non–Abelian corrections associated with the Berry curvature. In this sense, what collapses to a single exponential in the Abelian case becomes, for sequential decays, a correlated family of form factors governed by a non–Abelian holonomy.

A. Non-Abelian structure of the sequential holonomy

Since only two hadronic channels are relevant, the holonomy acts on a two-dimensional internal space, making it natural to regard the slope matrices R_1 and R_2 as elements of the Lie algebra $\mathfrak{su}(2)$. Accordingly one may write

$$R_1 = \vec{r}_1 \cdot \vec{\sigma}, \qquad R_2 = \vec{r}_2 \cdot \vec{\sigma}, \tag{30}$$

where $\vec{\sigma} = (\sigma_1, \sigma_2, \sigma_3)$ are the Pauli matrices and the real vectors $\vec{r}_1$ and $\vec{r}_2$ encode both the slopes and the mixing between the two channels. The non-Abelian nature of the problem becomes completely transparent, since

$$[R_1, R_2] = 2i\, (\vec{r}_1 \times \vec{r}_2) \cdot \vec{\sigma}, \tag{31}$$

so that the Berry curvature is directly proportional to the vector product $\vec{r}_1 \times \vec{r}_2$ in this internal space.

To leading orders in $(w_1 - 1)$ and $(w_2 - 1)$, the holonomy may be written as

$$\hat{\Xi}(w_1, w_2) \simeq \exp\!\left[-(w_1 - 1)\,\vec{r}_1 \cdot \vec{\sigma} - (w_2 - 1)\,\vec{r}_2 \cdot \vec{\sigma} \right] + \cdots, \tag{32}$$

which is again an element of $SU(2)$. Any traceless Hermitian 2×2 matrix can be written as $\vec{\alpha} \cdot \vec{\sigma}$ for some real vector $\vec{\alpha}$, and in the present case one finds

$$\vec{\alpha}(w_1, w_2) := (w_1 - 1)\,\vec{r}_1 + (w_2 - 1)\,\vec{r}_2. \tag{33}$$

The holonomy therefore has two eigenvalues,

$$\Xi_\pm(w_1, w_2) = \exp\!\big(\mp\, |\vec{\alpha}(w_1, w_2)| \big), \tag{34}$$

with invariant modulus

$$|\vec{\alpha}(w_1, w_2)|^2 = (w_1 - 1)^2 |\vec{r}_1|^2 + (w_2 - 1)^2 |\vec{r}_2|^2 + 2(w_1 - 1)(w_2 - 1)\,\vec{r}_1 \cdot \vec{r}_2. \tag{35}$$

These eigenvalues define two "geometric" Isgur-Wise functions which reduce to unity at zero recoil and generalise the familiar exponential law $\exp[-\rho^2(w - 1)]$ of the abelian case. They are not independent: both the slopes (controlled by $|\vec{r}_1|$ and $|\vec{r}_2|$) and their geometric interference (through the angle between $\vec{r}_1$ and $\vec{r}_2$) follow from the same underlying non-Abelian holonomy.

A convenient parametrisation is obtained by writing

$$\vec{r}_1 = \rho_1\, \hat{n}_1, \qquad \vec{r}_2 = \rho_2\, \hat{n}_2,$$

with unit vectors $\hat{n}_i$ and slopes $\rho_i = |\vec{r}_i|$. The geometric interference is encoded in the inner product $\hat{n}_1 \cdot \hat{n}_2 = \cos\theta$, where θ is the non-Abelian mixing angle between the two recoil directions.

With this parametrisation the holonomy eigenmodes are

$$\Xi_{\pm}(w_1, w_2) = \exp\left[\mp \sqrt{\rho_1^2(w_1 - 1)^2 + \rho_2^2(w_2 - 1)^2 + 2\rho_1\rho_2 \cos\theta \,(w_1 - 1)(w_2 - 1)}\right].$$

Physical Isgur–Wise functions correspond to the projections of $\hat{\Xi}(w_1, w_2)$ onto specific hadronic channels and therefore take the generic form

$$\xi_k(w_1, w_2) = c_k \, \Xi_{+}(w_1, w_2) + s_k \, \Xi_{-}(w_1, w_2),$$

where the coefficients (c_k, s_k) encode the channel-dependent projection angles determined by heavy–quark symmetry.

This provides a compact and physically transparent non-Abelian extension of the exponential parametrisation to sequential decays.

To the best of our knowledge, such a non-Abelian holonomic structure for sequential heavy-quark transitions has not been identified before in HQET or in nonperturbative treatments of QCD.

B.   Physical and phenomenological consequences

The explicit eigenvalues (34) uncover several qualitative and quantitative departures from the conventional HQET framework. The most important one is conceptual:

(1) Two universal geometric modes instead of a single form factor.
The non-Abelian holonomy associated with the broken recoil path possesses *two* universal eigenmodes $\Xi_{\pm}$, reflecting the underlying SU(2) structure of the infrared Berry connection. Physical Isgur–Wise functions are not independent scalar objects; rather, every hadronic channel corresponds to a fixed linear combination,

$$\Xi_{\text{phys}}^{(k)}(w_1, w_2) = A_{+}^{(k)} \, \Xi_{+}(w_1, w_2) + A_{-}^{(k)} \, \Xi_{-}(w_1, w_2), \tag{36}$$

so that all channels are correlated through the same universal geometric structure. This is a striking departure from HQET, where each channel has its own independent form factor at leading order.

(2) An emergent metric on the recoil plane.
The quantity

$$|\vec{\alpha}(w_1, w_2)|^2 = \delta w_a \, G_{ab} \, \delta w_b, \qquad G_{ab} = \vec{r}_a \cdot \vec{r}_b,$$

defines an effective metric on the (w_1, w_2) recoil plane. This metric encodes how the two recoil directions mix geometrically. The off-diagonal term $(w_1 - 1)(w_2 - 1)\,\vec{r}_1 \cdot \vec{r}_2$ represents interference between the two recoil steps and is controlled by the Berry curvature,

$$[R_1, R_2] \;\propto\; \vec{r}_1 \times \vec{r}_2.$$

Such mixing is *impossible* in conventional HQET, where the form factor for $B \to D^{**}$ depends independently on each recoil variable.

(3) Predictive correlations across hadronic channels.

The projection coefficients are

$$A_+^{(k)} = \cos^2(\gamma_k/2), \qquad A_-^{(k)} = \sin^2(\gamma_k/2), \tag{37}$$

with the angle γ_k determined by

$$\cos\gamma_k = \frac{\vec{s}_k \cdot \vec{\alpha}}{|\vec{\alpha}|}, \tag{38}$$

where each channel k is characterised by a fixed Bloch vector $\vec{s}_k$.

Thus, the physical Isgur–Wise functions are fixed geometrically by the alignment between:

(i) the channel vector $\vec{s}_k$, and (ii) the SU(2) holonomy direction $\hat{n} = \vec{\alpha}/|\vec{\alpha}|$.

This has immediate phenomenological implications:

- Channels with orthogonal vectors $(\vec{s}_k \cdot \hat{n} = 0)$ are *geometrically suppressed*.

- Channels aligned with the holonomy direction $(\vec{s}_k \parallel \hat{n})$ are *geometrically enhanced*.

- All channels share the *same* eigenmodes $\Xi_\pm$, so their slopes and curvatures are not independent but must satisfy definite geometric relations.

Such cross-channel constraints simply do not exist in HQET, where each transition is governed by its own unrelated form factor.

(4) Nontrivial kinematic patterns in the (w_1, w_2) plane.

Because $|\vec{\alpha}(w_1, w_2)|$ encodes the intrinsic geometry of the infrared holonomy, the sequential decay probes a two-dimensional structure not present in single–recoil transitions. This leads to:

- Correlated slopes in (w_1, w_2),

- Distinctive curvature patterns,

- Interference effects controlled by the Berry curvature,

27

- Angular distortions arising from the SU(2) structure.

All of these are experimentally testable in $B \to D^{**}\ell\nu$, $B \to D^{**}\tau\nu$, and $B \to D^{(*)}\pi\ell\nu$.

Sequential decays do not simply generalise the single-channel Isgur–Wise function; they reveal a genuinely non-Abelian geometric structure encoded in the SU(2) holonomy of the dressed heavy–light system. The appearance of two universal eigenmodes, the emergence of an effective metric on the recoil plane, and the interference effects driven by the Berry curvature represent new physics beyond HQET. The resulting correlated form factors provide a distinctive and testable prediction of the geometric, topologically structured infrared regime of QCD.

XI. NON-ABELIAN GEOMETRIC CONSTRAINTS BEYOND HQET

Once the projection coefficients $A_\pm^{(k)}$ are known explicitly as $\cos^2(\gamma_k/2)$ and $\sin^2(\gamma_k/2)$, the contrast with HQET becomes fully quantitative. In HQET every channel carries its own independent Isgur-Wise function, subject only to $\xi(1) = 1$ and $\xi'(1) = -\rho^2$, and sequential decays are treated as two unrelated transitions. Nothing in that framework correlates the slopes, curvatures, or shapes of the form factors associated with intermediate states.

In the present geometric approach, by contrast, the entire structure of the sequential decay is fixed by the non-Abelian holonomy and the channel-dependent angle γ_k defined through $\cos\gamma_k = (\vec{s}_k \cdot \vec{\alpha})/|\vec{\alpha}|$. All physical form factors follow from the same two universal eigenmodes $\Xi_\pm$, with no additional dynamical input. The physical Isgur-Wise functions therefore take the form

$$\Xi_{\text{phys}}^{(k)}(w_1, w_2) = \cos^2\frac{\gamma_k}{2}\, \Xi_+(w_1, w_2) + \sin^2\frac{\gamma_k}{2}\, \Xi_-(w_1, w_2), \tag{39}$$

which makes the dependence on the geometric data $(\vec{r}_1, \vec{r}_2)$ and on the intrinsic orientation $\vec{s}_k$ completely explicit. This leads to three sharpened departures from the HQET picture:

(i) **Channel-dependent correlated slopes:** Since $\Xi_\pm$ share the same recoil dependence, the slopes and curvatures of $\Xi_{\text{phys}}^{(k)}$ are determined solely by the angle γ_k. Different hadronic states thus obey nontrivial relations fixed by $\vec{s}_k$ and by the geometry of the recoil plane. Such cross-channel constraints cannot arise in HQET, even with additional parameters.

(ii) **Structured interference between recoil directions:** The mixed term $(w_1 - 1)(w_2 - 1)\,\vec{r}_1 \cdot \vec{r}_2$ enters each channel weighted by the projection $\vec{s}_k \cdot \hat{n}$, producing channel-dependent

modulations of angular and kinematical distributions. This refined pattern of interference is absent in HQET, where the two recoils contribute independently.

(iii) **Berry curvature contributions controlled by $\vec{s}_k$:** The commutator $[R_1, R_2] \propto \vec{r}_1 \times \vec{r}_2$ generates a Berry curvature whose physical impact is governed by the component of $\vec{s}_k$ perpendicular to the recoil plane. This produces characteristic distortions in the (w_1, w_2) distribution, again correlating channels in a way that HQET cannot reproduce.

XII.   SEQUENTIAL DECAYS $B \to D^{**} \to D$: GEOMETRIC PREDICTIONS

Sequential channels such as

$$B \to D^{**}(v') \to D(v'')$$

provide an ideal setting to test the non–Abelian geometric structure of the holonomy. Let $w_1 = v \cdot v'$ and $w_2 = v' \cdot v''$ be the two recoil variables, and define the geometric vector $\vec{\alpha}(w_1, w_2) = (w_1 - 1)\vec{r}_1 + (w_2 - 1)\vec{r}_2$. For any hadronic channel k with Bloch vector $\vec{s}_k$, the physical Isgur–Wise function takes the explicit form

$$\Xi_{\text{phys}}^{(k)}(w_1, w_2) = \cos^2\frac{\gamma_k}{2}\, \Xi_+(w_1, w_2) + \sin^2\frac{\gamma_k}{2}\, \Xi_-(w_1, w_2), \qquad \cos\gamma_k = \frac{\vec{s}_k \cdot \vec{\alpha}}{|\vec{\alpha}|}. \tag{40}$$

Thus the dependence on the channel k is entirely encoded in the geometric angle γ_k between $\vec{s}_k$ and the recoil direction $\hat{n} = \vec{\alpha}/|\vec{\alpha}|$.

a.   Correlated form factors.   In HQET the slopes of form factors involving different D^{**} states are independent phenomenological parameters. Here, however, the slope at zero recoil follows from

$$\rho_{(k)}^2 = -\left.\frac{\partial}{\partial w_1}\Xi_{\text{phys}}^{(k)}(w_1, w_2)\right|_{w_1 = w_2 = 1} = \cos\gamma_k \left.\frac{\partial}{\partial w_1}|\vec{\alpha}|\right|_{w_1 = w_2 = 1} + \cdots, \tag{41}$$

where the omitted terms involve derivatives of the universal eigenmodes $\Xi_\pm$. The key point is that $\rho_{(k)}^2$ depends only on the geometric data $(\vec{r}_1, \vec{r}_2)$ and the channel orientation $\vec{s}_k$; the slopes for different D^{**} states are therefore *not independent*, but obey definite geometric relations. Such correlations cannot be generated in HQET.

b.   Nontrivial w_1–w_2 structure.   The eigenvalues $\Xi_\pm$ depend on the norm $|\vec{\alpha}|$, which contains the interference term $(w_1 - 1)(w_2 - 1)\,\vec{r}_1 \cdot \vec{r}_2$. This produces a curved geometry in the (w_1, w_2) plane: the level sets of $\Xi_{\text{phys}}^{(k)}$ are no longer straight lines but nonlinear contours reflecting the un-

derlying SU(2) metric. These structures provide a direct, model–independent test of the geometric framework.

c.   Angular correlations.   Because the intermediate D^{**} state carries spin, the Berry curvature $[R_1, R_2] \propto \vec{r}_1 \times \vec{r}_2$ induces channel-dependent rotations in the internal SU(2) space. The strength of this effect is fixed by the component of $\vec{s}_k$ perpendicular to the recoil plane, leading to characteristic modifications of the helicity structure of the decay. These signatures persist in the heavy–quark limit and are potentially observable in high-statistics measurements at Belle II [28, 47] and LHCb [30, 42, 48].

XIII.   RELATION TO BJORKEN AND URALTSEV SUM RULES

In HQET, the Bjorken [49] and Uraltsev [50] sum rules constrain slopes and transition amplitudes by invoking the completeness of an infinite tower of intermediate excited states. In the geometric formulation developed here, the same logical role is played by the unitarity of the SU(2) holonomy. Since all physical Isgur-Wise functions are projections

$$\Xi_{\text{phys}}^{(k)} = \cos^2\frac{\gamma_k}{2}\,\Xi_+ + \sin^2\frac{\gamma_k}{2}\,\Xi_-,$$

with $\cos\gamma_k = (\vec{s}_k \cdot \vec{\alpha})/|\vec{\alpha}|$, the completeness of channels becomes the geometric identity

$$\sum_k \left(\cos^2\frac{\gamma_k}{2} + \sin^2\frac{\gamma_k}{2} \right) = 1, \tag{42}$$

which is nothing but the resolution of the identity for SU(2) doublets. Thus the analogue of Bjorken's sum rule emerges directly from the normalization of the Bloch vectors $\vec{s}_k$ rather than from a dynamical tower of excited states.

A similar statement holds for derivatives: geometric completeness implies relations among the slopes of the various channels,

$$\sum_k \rho_{(k)}^2 = \sum_k \cos\gamma_k \left. \frac{\partial}{\partial w_1}|\vec{\alpha}(w_1, w_2)| \right|_{w_1=w_2=1} + \cdots, \tag{43}$$

which generalise the Bjorken-Uraltsev constraints while remaining entirely independent of the HQET excitation spectrum. All departures from HQET sum rules arise from the geometric data: the effective metric G_{ab} and the Berry curvature $[R_1, R_2] \propto \vec{r}_1 \times \vec{r}_2$. The latter contributes corrections that vanish only in the abelian limit $[R_1, R_2] = 0$, thereby providing a transparent interpretation of observed deviations in transitions involving D^{**} intermediate states.

XIV. PHENOMENOLOGY OF THE TWO GEOMETRIC MODES

The two eigenmodes $\Xi_\pm$ represent the universal geometric responses of the dressed heavy–light system under adiabatic transport. Because any physical form factor is a superposition

$$\Xi^{(k)}_{\mathrm{phys}} = \cos^2\frac{\gamma_k}{2}\,\Xi_+ + \sin^2\frac{\gamma_k}{2}\,\Xi_-, \qquad \cos\gamma_k = \vec{s}_k\cdot\hat{n},$$

with $\hat{n} = \vec{\alpha}/|\vec{\alpha}|$, the angle γ_k fully determines how a given hadronic channel probes the two geometric modes.

a.   Interpretation of the modes.   The mode Ξ_+ corresponds to transport along the direction of minimal geometric response, in the sense that it exhibits the slowest variation with recoil. Conversely, Ξ_- represents the mode of maximal geometric response, displaying the steepest recoil behaviour. These two modes capture the complete non–Abelian content of the holonomy.

b.   Channel dependence and suppressions.   The coefficients $\cos^2(\gamma_k/2)$ and $\sin^2(\gamma_k/2)$ quantify the alignment of the hadronic Bloch vector $\vec{s}_k$ with the geometric direction $\hat{n}$: channels with $\gamma_k \approx 0$ are dominated by Ξ_+, while channels with $\gamma_k \approx \pi$ are dominated by Ξ_-. This explains, without additional model assumptions, why some D^{**} transitions are strongly suppressed while others display enhanced recoil sensitivity.

c.   Slopes and curvature.   Because Ξ_+ varies more slowly than Ξ_-, the slope and curvature of $\Xi^{(k)}_{\mathrm{phys}}$ are controlled directly by the value of γ_k. Channels dominated by Ξ_- (large γ_k) exhibit steeper slopes and enhanced curvature in the (w_1, w_2) plane, whereas channels dominated by Ξ_+ (small γ_k) produce flatter profiles. These geometric predictions have no analogue in HQET, where form–factor slopes are independent phenomenological inputs.

XV.   CONFRONTATION WITH BELLE, BELLE II, AND LHCB DATA

Current experimental data already contain enough information to test the geometric framework in a quantitatively meaningful and essentially model–independent way. Belle [27] and Belle II [28] provide high–statistics measurements of $B \to D^{**}\ell\nu$, including recoil and angular distributions that can be organised as a joint density in the two recoil variables (w_1, w_2). LHCb [30, 42, 48] offers complementary constraints through hadronic D^{**} decays and a precise determination of the composition and relative weights of the intermediate states.

In the geometric formulation, each physical form factor is an explicit projection of the SU(2)

holonomy,

$$\Xi_{\text{phys}}^{(k)}(w_1, w_2) = \cos^2\frac{\gamma_k}{2}\, e^{-|\vec{\alpha}(w_1,w_2)|} + \sin^2\frac{\gamma_k}{2}\, e^{+|\vec{\alpha}(w_1,w_2)|}, \qquad \cos\gamma_k = \frac{\vec{s}_k \cdot \vec{\alpha}(w_1, w_2)}{|\vec{\alpha}(w_1, w_2)|}, \qquad (44)$$

where

$$\vec{\alpha}(w_1, w_2) = (w_1 - 1)\,\vec{r}_1 + (w_2 - 1)\,\vec{r}_2,$$
$$|\vec{\alpha}(w_1, w_2)| = \sqrt{(w_1 - 1)^2|\vec{r}_1|^2 + (w_2 - 1)^2|\vec{r}_2|^2 + 2(w_1 - 1)(w_2 - 1)\,|\vec{r}_1||\vec{r}_2|\cos\theta}. \qquad (45)$$

and

$$\cos\theta = \frac{\vec{r}_1 \cdot \vec{r}_2}{|\vec{r}_1||\vec{r}_2|}.$$

Thus, all recoil dependence is encoded in the three geometric parameters $|\vec{r}_1|$, $|\vec{r}_2|$ and θ.

For a given hadronic channel k, the double–differential rate can be written schematically as

$$\frac{d^2\Gamma_k}{dw_1\, dw_2} = \mathcal{N}_k\, \mathcal{L}_k(w_1, w_2)\, \left|\Xi_{\text{phys}}^{(k)}(w_1, w_2)\right|^2, \qquad (46)$$

where $\mathcal{L}_k(w_1, w_2)$ is the known leptonic–kinematic factor and $\mathcal{N}_k$ collects normalisation constants and CKM factors. The entire nontrivial hadronic structure is therefore captured by the geometric form factor (44).

Experimentally, Belle, Belle II and LHCb provide:

- differential distributions $d\Gamma_k/dw$ for individual D^{**} channels (or appropriate projections of $d^2\Gamma_k/dw_1 dw_2$);

- angular distributions that separate helicity contributions and interference terms;

- fits to the relative fractions of $j = 1/2$ and $j = 3/2$ components and the composition of the D^{**} spectrum.

Within the geometric model, a combined fit to these observables proceeds in two conceptually clean steps:

1. *Extraction of the geometric recoil parameters.* Using the measured shapes of the distributions in (w_1, w_2) for a set of channels, one fits the three parameters $|\vec{r}_1|$, $|\vec{r}_2|$ and θ entering $|\vec{\alpha}(w_1, w_2)|$ in Eq. (45). This step is common to *all* channels.

2. *Determination of the channel angles γ_k.* Once $(|\vec{r}_1|, |\vec{r}_2|, \theta)$ are fixed, the only remaining freedom is the geometric angle γ_k that characterises each heavy–light configuration. The shape and normalisation of $d^2\Gamma_k/dw_1 dw_2$ then determine γ_k through Eq. (44).

In this way, the geometric framework makes the following concrete, testable predictions:

(i) **Curved level sets in the (w_1, w_2) plane.** Because $|\vec{\alpha}(w_1, w_2)|$ is a *nonlinear* function of the two recoils, level curves of the decay rate $\Gamma_k(w_1, w_2)$ follow curved contours determined by Eq. (45). Factorised parametrisations that depend only on linear combinations such as $a(w_1 - 1) + b(w_2 - 1)$ would instead produce approximately straight level sets. A two–dimensional analysis of Belle/Belle II data can directly discriminate between these behaviours.

(ii) **Correlated slopes between different D^{**} channels.** The slope of $\Xi_{\text{phys}}^{(k)}$ along, say, w_1 at zero recoil is fixed by the same $|\vec{r}_1|$ for all channels, and differs only by the angle γ_k. Explicitly,

$$\left. \frac{\partial \Xi_{\text{phys}}^{(k)}}{\partial w_1} \right|_{w_1 = w_2 = 1} = -|\vec{r}_1| \cos \gamma_k.$$

Thus, once one channel has been used to determine $|\vec{r}_1|$, the slopes of all other channels are fixed up to a cosine factor. Any pattern of uncorrelated or freely tunable slopes would contradict the geometric picture.

(iii) **Distinct helicity patterns induced by Berry curvature.** The commutator

$$[R_1, R_2] = 2i(\vec{r}_1 \times \vec{r}_2) \cdot \vec{\sigma}$$

measures the non–Abelian Berry curvature in the SU(2) space. Its component transverse to the recoil plane induces specific distortions in angular distributions and helicity amplitudes. These can be isolated experimentally in the angular analyses performed by Belle, Belle II and LHCb.

(iv) **Universal behaviour for channels with similar γ_k.** Channels whose Bloch vectors $\vec{s}_k$ make similar angles γ_k with $\hat{n}$ share the same mixture of the two geometric modes $\Xi_{\pm}$. This implies parameter–free relations between their shapes and ratios, which can be confronted with data across different D^{**} channels.

A dedicated global fit to Belle, Belle II and LHCb data using the explicit expression (44) would thus allow the extraction of the geometric parameters $(|\vec{r}_1|, |\vec{r}_2|, \theta)$ and the angles γ_k, providing a direct and quantitative test of the non–Abelian infrared structure encoded in the holonomy.

XVI. FALSIFIABLE PREDICTIONS

The geometric framework leads to a set of sharp, falsifiable predictions that follow directly from the SU(2) holonomy structure

$$\Xi_{\text{phys}}^{(k)} = \cos^2\frac{\gamma_k}{2}\,\Xi_+ + \sin^2\frac{\gamma_k}{2}\,\Xi_-, \qquad \Xi_\pm = e^{\mp|\vec{\alpha}|}, \qquad \cos\gamma_k = \frac{\vec{s}_k\cdot\vec{\alpha}}{|\vec{\alpha}|}.$$

(i) **Only two universal eigenmodes.** All heavy–quark channels must be linear combinations of the same two functions Ξ_+ and Ξ_-, with weights determined solely by the angles γ_k. Any statistically significant evidence for a third independent functional shape in the recoil dependence would rule out the holonomy picture.

(ii) **Explicit correlations of slopes and curvatures across channels.** Expanding near $(w_1, w_2) = (1, 1)$, one finds

$$\Xi_\pm(w_1, w_2) \simeq 1 \mp |\vec{\alpha}(w_1, w_2)| + \mathcal{O}((w-1)^2),$$

and therefore

$$\left.\frac{\partial\Xi_{\text{phys}}^{(k)}}{\partial w_1}\right|_{1,1} = -\,|\vec{r}_1|\cos\gamma_k, \qquad \left.\frac{\partial\Xi_{\text{phys}}^{(k)}}{\partial w_2}\right|_{1,1} = -\,|\vec{r}_2|\cos\gamma_k. \tag{47}$$

Once $|\vec{r}_1|$ and $|\vec{r}_2|$ are fixed by a reference channel, all other slopes are predicted up to the cosine of a single angle γ_k. Likewise, the mixed second derivatives are fixed by the interference term in $|\vec{\alpha}|$:

$$\left.\frac{\partial^2|\vec{\alpha}|^2}{\partial w_1\,\partial w_2}\right|_{1,1} = 2|\vec{r}_1||\vec{r}_2|\cos\theta,$$

showing that the non–factorisable curvature in the (w_1, w_2) plane is entirely controlled by θ. Any pattern of slopes and curvatures inconsistent with these relations would falsify the model.

(iii) **Intrinsically non–factorisable recoil geometry.** The dependence on w_1 and w_2 enters through $|\vec{\alpha}(w_1, w_2)|$, which contains the mixed term $(w_1 - 1)(w_2 - 1)\vec{r}_1\cdot\vec{r}_2$. Consequently, the decay surface in the (w_1, w_2) plane cannot be factorised into a product of a pure w_1 function times a pure w_2 function. Observation of level sets compatible with a factorised ansatz would be incompatible with the SU(2) holonomy interpretation.

(iv) **Helicity distortions controlled by Berry curvature.** The non–Abelian commutator

$$[R_1, R_2] = 2i(\vec{r}_1 \times \vec{r}_2)\cdot\vec{\sigma}$$

34

encodes the Berry curvature in the internal SU(2) space. Its magnitude and direction determine channel–dependent modifications of angular distributions and helicity amplitudes, in particular those that couple to helicity–flip structures in tauonic decays. High–statistics analyses that found no trace of these correlated distortions would directly refute the predicted non–Abelian structure.

Taken together, these signatures render the geometric model empirically testable. The sequential–decay analysis shows that the infrared sector of QCD, once rephrased in terms of adiabatic holonomies, imposes nontrivial geometric constraints linking different heavy–quark channels—constraints that are absent in conventional HQET.

Future extensions include multi–step cascades, nonleptonic transitions, and lattice determinations of the geometric vectors $\vec{r}_1$ and $\vec{r}_2$. In this broader perspective, the geometric framework offers a unified language connecting infrared QCD, Berry phases, and heavy–quark phenomenology in a way that goes beyond the standard HQET paradigm.

XVII.   THE 3/2 VS. 1/2 PUZZLE REVISITED

Before reviewing the heavy-quark expectations, it is useful to state clearly the long–standing problem that motivates this discussion. In the heavy–quark limit, HQET makes a robust prediction for semileptonic transitions into the $L = 1$ excited charmed mesons: the narrow $j = 3/2$ doublet should dominate the rate, while the broad $j = 1/2$ states are expected to be strongly suppressed. This hierarchy follows from well–understood angular–momentum selection rules and from the behaviour of the corresponding Isgur-Wise functions, $\tau_{3/2}(w)$ and $\tau_{1/2}(w)$, near zero recoil [51, 52].

Experimentally, however, the situation is markedly different. Measurements by Belle, BaBar, Belle II, LHCb, and earlier by CLEO indicate sizeable branching fractions into the broad $j = 1/2$ states, sometimes comparable to—or even exceeding—those into the $j = 3/2$ channels. This discrepancy, known as the "1/2 vs. 3/2 puzzle", was already evident in the first high–statistics Belle analysis [53] and subsequently confirmed by BaBar [54]. Despite numerous theoretical efforts-including $1/m_Q$ corrections, finite–width effects, improved form-factor parametrisations, and refined sum–rule analyses—no consensus has emerged.

The purpose of this section is to revisit the puzzle within the geometric framework developed in

this work. By interpreting the $B \to D^{**}$ transition as a process governed by Berry holonomies in the space of gauge configurations, the two $L = 1$ doublets acquire a natural and intrinsically non-Abelian description. As we shall show, this approach not only reproduces the qualitative HQET features but also explains, in a unified way, the correlated behaviour of the $j = 1/2$ and $j = 3/2$ form factors.

A. HQET expectations for $L = 1$ excitations

Heavy–quark effective theory yields a remarkably simple classification of the $L = 1$ excitations of the $D^{(*)}$ system. In the heavy–quark limit, the light degrees of freedom carry

$$j = \ell + s_{\text{light}}, \qquad \ell = 1, \quad s_{\text{light}} = \tfrac{1}{2},$$

leading to two doublets:

$$j = \tfrac{1}{2}: \quad D_0^*(0^+), \ D_1(1^+), \tag{48}$$

$$j = \tfrac{3}{2}: \quad D_1(1^+), \ D_2^*(2^+). \tag{49}$$

The semileptonic amplitudes for $B \to D^{**} \ell \nu$ are governed by two Isgur–Wise functions, $\tau_{1/2}(w)$ and $\tau_{3/2}(w)$ [51, 52]. At leading order, angular momentum selection rules imply

$$\tau_{1/2}(1) = 0, \qquad \tau_{3/2}(1) \neq 0,$$

up to $1/m_Q$ effects. Since phase space strongly weights the near–zero–recoil region, HQET predicts

$$\Gamma(B \to D^{**}_{j=3/2} \ell \nu) \ \gg \ \Gamma(B \to D^{**}_{j=1/2} \ell \nu), \tag{50}$$

namely that the $j = 3/2$ channels dominate the inclusive rate.

B. Experimental pattern and the $1/2$ vs. $3/2$ puzzle

The data tell a different story. Analyses by Belle [27, 37], BaBar [29, 36, 54], Belle II [28, 47], and LHCb [30, 42, 48] show that the broad $j = 1/2$ states are not suppressed but contribute at a level comparable to the $j = 3/2$ channels, sometimes even exceeding them. The observed pattern therefore contradicts the HQET hierarchy in Eq. (50).

From the HQET perspective this is unsurprising: at leading order the two functions are independent, and subleading corrections introduce further independent structures. HQET provides

36

no principle correlating slopes, curvatures, or angular dependencies of $\tau_{1/2}$ and $\tau_{3/2}$, nor relating them through any geometric constraint. This structural limitation is precisely what the geometric approach overcomes.

C. Geometric reinterpretation: explicit form of the two Isgur–Wise functions

Within the geometric framework, the transition is governed by a non-Abelian holonomy in the two-dimensional infrared space associated with the brown muck,

$$\hat{\Xi}(w_1, w_2) = \mathcal{P} \exp\Big[-(w_1 - 1)R_1 - (w_2 - 1)R_2 \Big],$$

where the "slope matrices"

$$R_1 = \vec{r}_1 \cdot \vec{\sigma}, \qquad R_2 = \vec{r}_2 \cdot \vec{\sigma},$$

encode the two independent recoil directions of the sequential process $B \to D^{**} \to D$. Their magnitudes and relative orientation,

$$\cos\theta = \frac{\vec{r}_1 \cdot \vec{r}_2}{|\vec{r}_1||\vec{r}_2|},$$

determine the geometric interference between the two deformations.

Near zero recoil the holonomy takes the closed form

$$\hat{\Xi}(w_1, w_2) = \exp\Big[-\vec{\alpha}(w_1, w_2) \cdot \vec{\sigma} \Big],$$

with effective recoil vector

$$\vec{\alpha}(w_1, w_2) = (w_1 - 1)\,\vec{r}_1 + (w_2 - 1)\,\vec{r}_2,$$

and norm

$$|\vec{\alpha}(w_1, w_2)| = \sqrt{(w_1 - 1)^2|\vec{r}_1|^2 + (w_2 - 1)^2|\vec{r}_2|^2 + 2(w_1 - 1)(w_2 - 1)\,|\vec{r}_1||\vec{r}_2|\cos\theta}.$$

Since any traceless Hermitian 2×2 matrix has eigenvalues $\pm|\vec{\alpha}|$, the two universal geometric modes are

$$\Xi_\pm(w_1, w_2) = \exp\Big[\mp\, |\vec{\alpha}(w_1, w_2)| \Big].$$

Projecting these modes onto the physical hadronic channels yields the two Isgur–Wise functions for the $L = 1$ excitations:

$$\tau_{3/2}(w_1, w_2) = \cos\frac{\gamma}{2}\,\Xi_+ + \sin\frac{\gamma}{2}\,\Xi_-, \tag{51}$$

$$\tau_{1/2}(w_1, w_2) = -\sin\frac{\gamma}{2}\,\Xi_+ + \cos\frac{\gamma}{2}\,\Xi_-, \tag{52}$$

where the Berry angle $\gamma = \gamma(\theta)$ depends solely on the relative orientation of the two recoil directions.

In this way:

1. The two IW functions are not independent: they are orthogonal projections of a single SU(2) holonomy. 2. Their slopes and curvatures are fixed by the geometric data $(|\vec{r}_1|, |\vec{r}_2|, \theta)$. 3. The correlated behaviour observed experimentally follows naturally from the holonomic structure.

The geometric framework therefore resolves the "1/2 vs. 3/2 puzzle": the two channels are not distinct dynamical mechanisms but different projections of the same non-Abelian adiabatic holonomy associated with the infrared dressing of the heavy–light system.

D. Geometric reinterpretation in terms of SU(2) holonomy

In the geometric formulation developed in this work, the sequential process $B \to D^{**} \to D$ is controlled not by two unrelated scalar form factors but by a *single* SU(2) holonomy acting on a two–dimensional internal space of heavy–light configurations. This non–Abelian structure is the natural analogue of the Wilczek–Zee geometric phase arising in multilevel adiabatic systems [55–57].

To make the construction explicit, consider the holonomy along the two independent recoil deformations (w_1, w_2):

$$\hat{\Xi}(w_1, w_2) = \exp\left[-\vec{\alpha}(w_1, w_2){\cdot}\vec{\sigma}\right], \qquad \vec{\alpha}(w_1, w_2) = (w_1 - 1)\,\vec{r}_1 + (w_2 - 1)\,\vec{r}_2. \qquad (53)$$

Here $\vec{r}_1$ and $\vec{r}_2$ are the slope vectors associated with the two recoil directions; their magnitudes set the slopes, while their relative orientation,

$$\cos\theta := \frac{\vec{r}_1 \cdot \vec{r}_2}{|\vec{r}_1||\vec{r}_2|},$$

encodes the geometric interference between them.

Since $\vec{\alpha}{\cdot}\vec{\sigma}$ is a traceless Hermitian matrix, it has eigenvalues $\pm|\vec{\alpha}|$, with normalised eigenvectors whose Bloch vectors point along the direction

$$\hat{n} = \frac{\vec{\alpha}}{|\vec{\alpha}|}.$$

Thus the holonomy admits the spectral decomposition

$$\hat{\Xi}(w_1, w_2) = \Xi_+(w_1, w_2)\,\Pi_+ + \Xi_-(w_1, w_2)\,\Pi_-, \qquad \Xi_\pm(w_1, w_2) = \exp\left[\mp |\vec{\alpha}(w_1, w_2)|\right], \qquad (54)$$

where

$$\Pi_\pm = \frac{1}{2}\left(\mathbf{1} \pm \hat{n}{\cdot}\vec{\sigma}\right)$$

38

are the projectors onto the two geometric eigenmodes of the infrared dressing.

The essential point is that *all* physical Isgur–Wise functions arise by projecting the universal object $\hat{\Xi}$ onto a channel–dependent SU(2) direction. Let $\vec{s}_k$ denote the Bloch vector representing channel k. Then

$$\Xi_{\text{phys}}^{(k)} = \langle \vec{s}_k \,|\, \hat{\Xi} \,|\, \vec{s}_k \rangle = \cos^2\frac{\gamma_k}{2}\,\Xi_+ + \sin^2\frac{\gamma_k}{2}\,\Xi_-,$$

where γ_k is the angle between $\vec{s}_k$ and the holonomy direction $\hat{n}$:

$$\cos\gamma_k = \vec{s}_k \cdot \hat{n}.$$

This gives Eq. (54) and makes the geometry fully explicit: physical channels differ only through the angle γ_k.

  a. Geometric meaning of γ_k. If $\gamma_k = 0$, the channel is aligned with the slow mode Ξ_+; if $\gamma_k = \pi$, it aligns with the fast mode Ξ_- and therefore inherits stronger variation with recoil. Intermediate angles interpolate smoothly between these behaviours.

  b. Explicit expression for the magnitude $|\vec{\alpha}|$. The dependence on the two recoil directions is

$$|\vec{\alpha}(w_1, w_2)| = \sqrt{(w_1 - 1)^2|\vec{r}_1|^2 + (w_2 - 1)^2|\vec{r}_2|^2 + 2(w_1 - 1)(w_2 - 1)\,|\vec{r}_1||\vec{r}_2|\cos\theta}. \tag{55}$$

This is the SU(2) generalisation of the single–slope exponential parametrisation used in $B \to D^{(*)}$.

E. Slope mixing and explicit derivatives at zero recoil

To illustrate how geometry controls the hierarchy, we compute explicitly the slope of $\Xi_{\text{phys}}^{(k)}$ with respect to one recoil variable. From Eq. (55),

$$\Xi_\pm(w_1, w_2) = \exp\big[\mp\,|\vec{\alpha}(w_1, w_2)|\big],$$

and differentiating at $(w_1, w_2) = (1, 1)$ gives

$$\Xi_\pm' := \frac{\partial \Xi_\pm}{\partial w_1}\bigg|_{1,1} = \mp\,|\vec{r}_1|\,\Xi_\pm(1, 1),$$

since $\vec{\alpha} = 0$ at zero recoil and $\partial_{w_1}|\vec{\alpha}|\,\big|_{1,1} = |\vec{r}_1|$.

The channel–dependent slope follows by projecting:

$$\frac{\partial \Xi_{\text{phys}}^{(k)}}{\partial w_1}\bigg|_{1,1} = \cos^2\frac{\gamma_k}{2}\,\Xi_+' + \sin^2\frac{\gamma_k}{2}\,\Xi_-', \tag{56}$$

which reproduces Eq. (56) but now with all intermediate steps made explicit.

Because $|\Xi'_-| > |\Xi'_+|$ (the $-$ mode varies more rapidly), channels with larger γ_k contain a larger admixture of the fast mode and therefore exhibit steeper slopes and enhanced curvature. The hierarchy across channels is thus controlled by the geometry of recoil, not by unrelated dynamical amplitudes.

F.   Geometric mechanism behind the hierarchy

In this language, the $3/2$ vs. $1/2$ puzzle becomes a statement about the relative orientation of the Bloch vectors $\vec{s}_{1/2}$ and $\vec{s}_{3/2}$. If the $j = 1/2$ doublet corresponds to a larger misalignment angle $\gamma_{1/2}$ than the $j = 3/2$ one, then

$$\Xi^{(1/2)}_{\text{phys}} \text{ receives more weight from the fast mode } \Xi_-,$$

and therefore varies more rapidly with recoil. This enhanced geometric response produces larger slopes and curvature and explains why $j = 1/2$ contributions to the rate can be sizeable even though HQET predicts a suppression based on angular–momentum selection rules alone.

HQET, which treats $\tau_{1/2}$ and $\tau_{3/2}$ as *independent* scalar objects, has no mechanism to correlate their behaviours. The geometric approach, by contrast, predicts such correlations automatically because both functions derive from the same SU(2) structure.

G.   Tauonic Channels as Enhanced Probes of Non–Abelian Geometry

Tauonic semileptonic decays provide a particularly sensitive arena for non–Abelian geometric effects. The large τ mass compresses the accessible kinematic domain toward $w = 1$ and enhances helicity–flip contributions that vanish for light leptons. Consequently, these channels probe precisely the region where the curvature of the holonomy is largest.

a.   Geometric sensitivity.   Using Eq. (54), even a modest increase in γ_k enhances the contribution from Ξ_-, which dominates the curvature near zero recoil. Since tauonic decays populate this region more densely, they respond strongly to small geometric misalignments that remain invisible in e and μ modes.

b.   Berry curvature and helicity structure.   The non–Abelian commutator

$$[R_1, R_2] = 2i(\vec{r}_1 \times \vec{r}_2) \cdot \vec{\sigma}$$

measures the Berry curvature of the infrared SU(2) connection. This curvature modulates precisely those components of the hadronic tensor that couple to helicity–flip structures in the leptonic current—structures which are suppressed for light leptons but survive for τ's. Thus, tauonic modes provide a direct probe of the non–Abelian infrared geometry.

c. Role of excited states. Broad $j = 1/2$ states are associated with larger angles γ_k and therefore with enhanced coupling to Ξ_-. This explains qualitatively why D^{**} contributions are more prominent in tauonic decays than in light–lepton modes, independently of specific dynamical models.

d. Correlated predictions. All channels—D, D^*, and D^{**}—derive from the same SU(2) holonomy. Thus the ratios $R(D)$, $R(D^*)$, and their D^{**} analogues are correlated in a manner impossible within HQET, which treats each channel with independent parameters. These correlations constitute distinctive predictions for Belle II.

XVIII. QUANTIZED FUNCTIONAL FLUX AND THE EMERGENCE OF NON-ABELIAN HOLONOMIES

The previous sections have shown that the Isgur–Wise function is naturally interpreted as a holonomy associated with the adiabatic motion of a heavy quark through the infrared gauge background. A structural property underlying this construction is the *quantization of the functional Berry flux* in the infrared sector of QCD.

The conventional geometric–phase framework [56–59] describes Berry curvature defined over finite–dimensional parameter spaces. However, in the present context the curvature is defined over the *functional space* of infrared gauge configurations. The resulting flux quantization is therefore a property of the infrared gauge sector itself, rather than of a level degeneracy in a few–level system. The integer that labels the flux corresponds to a topological infrared *sector* of the gauge field, and any realistic process probes an average over these sectors through the heavy–light cloud.

A. Functional Berry curvature and its quantized flux

Let $\mathcal{A}$ denote the Berry connection on the space of gauge configurations, defined by the adiabatic evolution of the dressed heavy–light state following the usual geometric principles [56, 60]. Its

curvature,

$$\mathcal{F} = d\mathcal{A} + \mathcal{A} \wedge \mathcal{A}, \tag{57}$$

encodes the response of the infrared cloud to variations of the external four–velocity and of the underlying gauge configuration.

Because the adiabatic manifold of dressed configurations contains noncontractible two–cycles Σ in the infrared, the curvature flux through such cycles is quantized:

$$\frac{1}{2\pi} \int_{\Sigma} \mathcal{F} = n \in \mathbb{Z}. \tag{58}$$

This is the functional analogue of the familiar quantization of Berry flux in quantum systems [56, 57], but in the present context it reflects the topology of the infrared gauge manifold of QCD. Equation (58) constrains the admissible holonomies and organises the infrared dynamics into topological sectors labelled by n. The holonomy of the dressed heavy–light system must then be built out of these quantized fluxes.

B. Consequences for abelian holonomies in $B \rightarrow D^{(*)}$

For transitions with a single recoil parameter, $w = v \cdot v'$, the motion in the adiabatic manifold is effectively one–dimensional, and the relevant projection of the Berry connection is abelian. In this situation the holonomy along the recoil trajectory can be written as

$$\Xi_{\mathrm{geom}}(w) = \exp\left[i \int_{C_w} \mathcal{A}_{\mathrm{eff}} \right], \tag{59}$$

where $\mathcal{A}_{\mathrm{eff}}$ is the effective abelian component of the Berry connection along the w–direction.

Flux quantization implies that this effective connection is not arbitrary: in each topological sector one has

$$\frac{1}{2\pi} \int_{\Sigma} \mathcal{F} = n, \qquad n \in \mathbb{Z}, \tag{60}$$

so that the holonomy accumulated between $w = 1$ and $w > 1$ is proportional to the integer n times a fixed geometric factor. To leading order in $(w-1)$, and in the regime in which a single topological sector dominates the adiabatic evolution, the holonomy takes the exponential form

$$\Xi_{\mathrm{geom}}(w) \simeq \exp[-(w-1)\rho^2], \qquad \rho^2 \propto \frac{1}{2\pi} \int_{\Sigma} \mathcal{F}, \tag{61}$$

where the proportionality factor depends on the detailed geometry of the infrared manifold but not on the microscopic composition of the cloud.

Thus, in the abelian case the exponential behaviour of $\Xi(w)$ is a structural consequence of the infrared geometry: the slope at zero recoil is fixed by the quantized flux, and once ρ^2 is determined experimentally the entire functional form near $w = 1$ follows from the underlying Berry connection. Different hadronic channels probe the same exponent, up to the usual normalisation factors.

C. Two-dimensional adiabatic motion and the emergence of SU(2)

Sequential transitions $B \to D^{**} \to D$ involve two independent recoil parameters, $w_1 = v \cdot v_1$ and $w_2 = v_1 \cdot v_2$, probing a two–dimensional region of the adiabatic manifold. In this situation the effective curvature $\mathcal{F}$ projected onto the (w_1, w_2) plane cannot be globally diagonalized, and the holonomy becomes genuinely non–abelian. While non–abelian parallel transport is familiar from quantum–mechanical systems [55], here its origin is the infrared geometry of QCD and, in particular, the quantized flux (58) in a two–dimensional subspace of the functional manifold.

Near zero recoil, the holonomy can be written as

$$\hat{\Xi}(w_1, w_2) = \mathcal{P} \exp\left[-(w_1 - 1)R_1 - (w_2 - 1)R_2 + \tfrac{1}{2}(w_1 - 1)(w_2 - 1)[R_1, R_2] + \cdots\right], \qquad (62)$$

where R_1 and R_2 are the geometric generators associated with the two recoil directions and $[R_1, R_2]$ measures the projected Berry curvature in the (w_1, w_2) plane.

Flux quantization now has a stronger consequence: it restricts the holonomy to a compact subgroup generated by R_1 and R_2. The minimal nontrivial representation compatible with a nonzero commutator $[R_1, R_2]$ is two–dimensional, and the corresponding compact group is SU(2) up to an overall phase. Equivalently, the infrared dynamics effectively selects a two–level geometric subspace in which the holonomy acts. In this subspace, the holonomy has two universal eigenmodes,

$$\Xi_\pm(w_1, w_2) = \exp[\mp |\vec{\alpha}(w_1, w_2)|], \qquad \vec{\alpha}(w_1, w_2) = (w_1 - 1)\vec{r}_1 + (w_2 - 1)\vec{r}_2, \qquad (63)$$

with $\vec{r}_1$ and $\vec{r}_2$ determined by the infrared Berry curvature.

All heavy–quark form factors in sequential decays can then be written as channel–dependent projections of these two universal modes:

$$F_k(w_1, w_2) = \cos^2\frac{\gamma_k}{2}\, \Xi_+(w_1, w_2) + \sin^2\frac{\gamma_k}{2}\, \Xi_-(w_1, w_2), \qquad (64)$$

where the angle γ_k encodes the SU(2) orientation of the corresponding heavy–light state.

D. Explicit consequences for sequential decays

The structure above has several experimentally testable implications:

- *Correlated slopes and curvatures.* The slopes of the form factors in the two recoil directions are governed by the same flux parameters and by the vectors $\vec{r}_1, \vec{r}_2$. As a result, different channels exhibit correlated slopes and curvatures in the (w_1, w_2) plane, rather than arbitrary shapes.

- *Curvature–induced interference.* The commutator term $[R_1, R_2]$ induced by the Berry curvature leads to characteristic interference patterns in sequential decays, including non-factorisable dependence on (w_1, w_2) and modified angular distributions in $D^{**} \to D\pi$. These features are consistent with the general structures expected in HQET analyses [24, 52, 61], but here they arise from a single geometric mechanism.

- *Universal eigenmodes and channel projections.* All channels are governed by the same two geometric modes $\Xi_\pm$, with channel–dependent weights determined by γ_k. This replaces the HQET picture of unrelated scalar form factors by a unified SU(2) holonomy, from which all physical Isgur–Wise functions are obtained as projections.

In summary, the non–abelian structure observed in sequential decays follows directly from the quantized functional flux of the infrared Berry curvature. The exponential Isgur–Wise form for $B \to D^{(*)}$ and the SU(2) holonomy structure for $B \to D^{**} \to D$ are two manifestations of the same topological organisation of the infrared sector of QCD.

E. Isospin violation in the $X(3872)$: Infrared Perspective

The exotic state $X(3872)$ provides one of the clearest examples in which threshold physics and infrared dynamics play a central role in organizing the hadronic state space. From a qualitative point of view, this system admits a natural analogy with molecular physics, in particular with the hydrogen molecule, suggesting a description based on a Born–Oppenheimer approximation.

Within this analogy, the heavy $c\bar{c}$ pair plays the role of the heavy nuclei, whose relative separation R defines a slow parameter. The light degrees of freedom –light quarks and gluons– adjust adiabatically to this separation, generating effective states that depend parametrically on R. When

the distance between the charm quark c and the antiquark $\bar{c}$ is large, the system behaves as an extended molecular state, while for smaller values of R it gradually approaches a more compact configuration, analogous to a conventional charmonium state.

At this stage, the molecular analogy by itself does not imply any violation of isospin. In the ideal limit of exact isospin symmetry, $m_u = m_d$, and in the absence of electromagnetic effects, the light sector admits adiabatic states with well–defined isospin, which therefore appears as a good quantum number of the system. This observation naturally raises a fundamental question: where does the exceptionally large isospin violation observed in the decays of the $X(3872)$ originate?

The crucial difference with ordinary molecular systems lies in the structure of the relevant adiabatic state space. In the case of the $X(3872)$, the infrared regime is dominated by two nearly degenerate channels associated with the $D^0\bar{D}^{*0}$ and D^+D^{*-} thresholds. These channels differ in their isospin content, yet they are separated by an extremely small energy scale. As a result, the light sector does not define a single, well–isolated adiabatic state, but rather a quasi-degenerate subspace of dimension greater than one.

This feature is particularly significant, as it reveals a deep analogy with molecular physics: the presence of a quasi–degeneracy implies, in an inevitable way, that the Berry connection associated with adiabatic transport is non-Abelian. Since the appearance of Berry phases constitutes a clear signal of non–perturbative physics, physical states must be interpreted in terms of infrared-dressed states generated by adiabatic transport in the functional configuration space $\mathcal{A}/\mathcal{G}$. In this framework, the associated adiabatic connection does not, in general, admit a global basis in which isospin remains well defined throughout the infrared evolution.

From this perspective, the isospin violation observed in the $X(3872)$ should not be interpreted as an accidental dynamical effect or as a simple consequence of small mass differences between charged and neutral channels. Rather, it emerges as a geometric effect tied to the structure of the infrared state space and to the quasi-degenerate character of the light sector. Isospin thus ceases to be a protected quantum number of the infrared physical Hilbert space, and its violation manifests itself as a collective property of the dressed state.

The goal of this work is to explore systematically this infrared functional interpretation of the $X(3872)$. Rather than proposing a new microscopic model, we focus on clarifying the geometric origin of isospin violation and on establishing the $X(3872)$ as a natural laboratory for studying how approximate symmetries may cease to provide reliable quantum labels in the infrared regime

of QCD.

To address this problem in a concrete setting, it is convenient to consider the $X(3872)$ in the context of sequential decays of B mesons. Schematically, the process can be written as

$$B \ \to \ A \ \to \ X, \tag{65}$$

where A denotes an effective intermediate state. This state should not be interpreted as a well–defined physical resonance, but rather as the projection of the decay process onto a quasi-degenerate subspace of the light sector that is relevant in the infrared regime.

Within this approach, instead of analyzing the decay in terms of spin channels, we focus on the evolution of the isospin degrees of freedom along the sequential process. The natural separation of scales characteristic of heavy–meson decays allows the heavy-quark spin to be treated as a spectator, while infrared dynamics governs the mixing of channels with different isospin content.

Since the $X(3872)$ decays into the final states $J/\psi\,\rho$ and $J/\psi\,\omega$, we may proceed in close analogy with the analysis of sequential decays discussed previously for an effective $SU(2)$ symmetry. In the present case, however, this structure does not act in the bidimensional recoil space, but rather in the isospin space associated with the $I = 1$ and $I = 0$ channels, respectively.

The coexistence of these two final states, which are quasi-degenerate in the infrared regime but differ in their isospin content, defines a natural two–dimensional subspace on which the adiabatic transport induced by the sequential decay acts. In this sense, the observed mixing between the $J/\psi\,\rho$ and $J/\psi\,\omega$ channels can be interpreted as the result of a non-Abelian holonomy in isospin space, fully analogous to the $SU(2)$ structure that emerges in the analysis of multiple recoils.

From this viewpoint, isospin violation is not introduced as an explicit breaking term in the dynamics, but rather arises as a geometric consequence of adiabatic transport in a quasi-degenerate subspace of the infrared physical state space. The formal parametrizations remain essentially unchanged; what changes in a substantial way is their physical interpretation. The same mathematical structures that describe dynamics in a bidimensional recoil space now act in isospin space, reflecting that the essential difference lies not in the form of the amplitudes, but in the physical meaning of the degrees of freedom involved.

The central issue clarified by this approach is therefore why isospin ceases to be a reliable quantum label in the $X(3872)$, even though the effective structure governing the evolution in the $(J/\psi\,\rho,\ J/\psi\,\omega)$ subspace is formally $SU(2)$-covariant. The answer does not lie in an explicit breaking

46

of the symmetry in the underlying dynamics, but in the infrared regime in which the state is formed. In the presence of a quasi-degenerate subspace dominated by infrared dynamics, physical states are defined by adiabatic transport and holonomies in configuration space, rather than by eigenstates of symmetry generators.

From this perspective, the $X(3872)$ does not represent an anomaly of isospin symmetry, but rather a paradigmatic example of how approximate symmetries may lose their significance as state labels in the quasi–degenerate infrared regime of QCD.

Our results are consistent with the pattern observed by Belle and LHCb, in particular with the presence of a large and robust isospin violation in the decays of the $X(3872)$. Within our framework, this behavior arises naturally as a consequence of infrared dynamics in a quasi-degenerate state space, without requiring any explicit breaking of isospin symmetry.

XIX.   CONCLUSIONS

The geometric reinterpretation developed in this work provides a conceptual, mathematical, and phenomenological refinement of the heavy–quark effective theory. By identifying the heavy–light system as an adiabatically dressed infrared object, the traditionally opaque structure of the "brown muck" acquires a precise meaning in terms of Berry phases and functional holonomies. Within this framework, heavy–quark symmetry emerges not as a dynamical simplification but as a statement of parallel transport in the infrared configuration space.

A key structural advancement of this work is the explicit recognition that the Berry curvature associated with the infrared cloud possesses a *quantized functional flux*. This quantization, made explicit in Sec. XVIII, fixes the holonomy class of the dressed heavy–light state and determines the admissible geometric phases. In processes with a single recoil parameter $(B \to D^{(*)})$, this leads to an abelian holonomy whose slope and global shape are not arbitrary but follow directly from the quantized flux. Once ρ^2 is fixed near zero recoil, the entire functional form of $\Xi(w)$ is determined by the underlying Berry connection, predicting a characteristic exponential falloff. This behaviour differs sharply from polynomial or truncated dispersive parametrisations and yields clean opportunities for experimental tests with the improved precision expected at Belle II.

When two independent recoil directions are probed—as in sequential decays $B \to D^{**} \to D$— the adiabatic motion explores a effectively two–dimensional region of configuration space. In this

47

regime the curvature cannot be diagonalized globally, and flux quantization forces the holonomy into an intrinsic SU(2) structure. All physical form factors in one–step and sequential transitions then arise as explicit projections of two universal geometric modes, with channel-dependent weights

$$A_+^{(k)} = \cos^2\frac{\gamma_k}{2}, \qquad A_-^{(k)} = \sin^2\frac{\gamma_k}{2},$$

determined by the orientation of the heavy–light state in the internal SU(2) space. The phenomenology of different D^{**} channels is therefore not independent: their slopes, curvatures, suppressions, and angular structures are linked by geometric relations involving the Bloch vectors $\vec{s}_k$ and the geometric recoil direction $\hat{n}$. Such cross–channel correlations cannot arise in HQET, where each form factor is an unconstrained scalar function.

The geometric structure also clarifies the origin and magnitude of $1/m_Q$ corrections. Departures from strict universality are governed by the effective metric $G_{ab} = \vec{r}_a \cdot \vec{r}_b$ and by the Berry curvature $[R_1, R_2] \propto \vec{r}_1 \times \vec{r}_2$. These quantities determine the non-factorisable curvature of the decay surface in the (w_1, w_2) plane, the correlated slopes across D^{**} channels, and distinctive modifications of helicity amplitudes. All these effects constitute falsifiable predictions of the geometric framework and lie within reach of high-statistics analyses at Belle II and LHCb.

From this perspective, several longstanding phenomenological tensions acquire a natural reinterpretation. The 1/2 vs. 3/2 puzzle, traditionally framed as a conflict between HQET expectations and experimental rates, emerges geometrically from the different orientations of the heavy–light states in the internal SU(2) space. Tauonic decays, which probe precisely the region where the curvature associated with the fast geometric mode is largest, become selective amplifiers of the non-Abelian geometric response and hence sensitive probes of the functional Berry curvature.

Overall, the adiabatic holonomy approach offers a coherent and predictive framework that unifies infrared QCD, Berry phases, and heavy–quark symmetry. It replaces the phenomenological freedom of HQET with a constrained geometric structure, correlates observables across channels, and yields distinctive predictions for recoil and angular distributions. Future comparisons with high-precision measurements will determine whether the anomalies observed in excited-channel transitions indeed reflect a non-Abelian infrared geometry, or whether additional dynamical ingredients are required. In either case, the geometric framework introduced here provides a systematic and conceptually transparent path for organising and interpreting the infrared dynamics of heavy–light hadrons.

Appendix A: Geometric derivation of the coefficients $A_\pm^{(k)}$

In this appendix we provide a brief derivation of the coefficients $A_\pm^{(k)}$ appearing in Eq. (36), using the SU(2) structure underlying the non–Abelian holonomy.

1. SU(2) holonomy and its eigenmodes

Recall that in the sequential decay the effective holonomy in the infrared sector can be written as

$$U(w_1, w_2) \simeq \exp\left[-\,\vec{\alpha}(w_1, w_2)\cdot\vec{\sigma}\right], \qquad \vec{\alpha}(w_1, w_2) = (w_1 - 1)\,\vec{r}_1 + (w_2 - 1)\,\vec{r}_2, \qquad \text{(A1)}$$

where $\vec{r}_a$ $(a = 1, 2)$ are fixed vectors in the internal SU(2) space and $\vec{\sigma}$ denotes the Pauli matrices. Defining the norm and unit vector

$$|\vec{\alpha}| := \left(\vec{\alpha}\cdot\vec{\alpha}\right)^{1/2}, \qquad \hat{n}(w_1, w_2) := \frac{\vec{\alpha}(w_1, w_2)}{|\vec{\alpha}(w_1, w_2)|}, \qquad \text{(A2)}$$

the holonomy can be recast as

$$U(w_1, w_2) = \exp\left[-\,|\vec{\alpha}|\,\hat{n}\cdot\vec{\sigma}\right]. \qquad \text{(A3)}$$

The operator $\hat{n}\cdot\vec{\sigma}$ has two eigenvalues ± 1 with eigenvectors $|\chi_\pm\rangle$:

$$\left(\hat{n}\cdot\vec{\sigma}\right)|\chi_\pm\rangle = \pm\,|\chi_\pm\rangle. \qquad \text{(A4)}$$

It follows immediately that

$$U(w_1, w_2)\,|\chi_\pm\rangle = \exp\left(\mp\,|\vec{\alpha}(w_1, w_2)|\right)|\chi_\pm\rangle =: \Xi_\pm(w_1, w_2)\,|\chi_\pm\rangle, \qquad \text{(A5)}$$

so that the two universal eigenvalues are

$$\Xi_\pm(w_1, w_2) = \exp\left(\mp\,|\vec{\alpha}(w_1, w_2)|\right). \qquad \text{(A6)}$$

The spectral decomposition of the holonomy then reads

$$U(w_1, w_2) = \Xi_+(w_1, w_2)\,|\chi_+\rangle\langle\chi_+| + \Xi_-(w_1, w_2)\,|\chi_-\rangle\langle\chi_-|. \qquad \text{(A7)}$$

2.   Physical form factors and projection coefficients

Let $|k\rangle$ denote the effective SU(2) doublet associated with a given hadronic channel k (for instance, a particular D^{**} state with fixed polarisation). In our construction, the physical Isgur–Wise function for channel k is defined as the expectation value of the holonomy,

$$\Xi^{(k)}_{\text{phys}}(w_1, w_2) := \langle k| \, U(w_1, w_2) \, |k\rangle . \tag{A8}$$

Using the spectral representation (A7) we obtain

$$\Xi^{(k)}_{\text{phys}}(w_1, w_2) = \Xi_+(w_1, w_2) \, |\langle k|\chi_+\rangle|^2 + \Xi_-(w_1, w_2) \, |\langle k|\chi_-\rangle|^2. \tag{A9}$$

Comparing with

$$\Xi^{(k)}_{\text{phys}}(w_1, w_2) = A^{(k)}_+ \, \Xi_+(w_1, w_2) + A^{(k)}_- \, \Xi_-(w_1, w_2), \tag{A10}$$

we immediately identify

$$A^{(k)}_+ = |\langle k|\chi_+\rangle|^2, \qquad A^{(k)}_- = |\langle k|\chi_-\rangle|^2, \tag{A11}$$

so that $A^{(k)}_+$ and $A^{(k)}_-$ are the probabilities to find the channel k in the geometric eigenmodes $|\chi_+\rangle$ and $|\chi_-\rangle$, respectively. As a consequence,

$$A^{(k)}_+ + A^{(k)}_- = 1. \tag{A12}$$

3.   Explicit expression in the Bloch representation

The coefficients $A^{(k)}_\pm$ can be made fully explicit by exploiting the Bloch representation of SU(2) states. The pure state $|k\rangle$ is described by a unit Bloch vector $\vec{s}_k$, with density matrix

$$\rho_k := |k\rangle\langle k| = \frac{1}{2}\left(\mathbb{1} + \vec{s}_k \cdot \vec{\sigma}\right), \qquad |\vec{s}_k| = 1. \tag{A13}$$

Similarly, the projectors onto the eigenvectors $|\chi_\pm\rangle$ of $\hat{n}\cdot\vec{\sigma}$ are

$$P_\pm := |\chi_\pm\rangle\langle\chi_\pm| = \frac{1}{2}\left(\mathbb{1} \pm \hat{n}\cdot\vec{\sigma}\right). \tag{A14}$$

Using Eq. (A11) we can write

$$A^{(k)}_\pm = \langle k| P_\pm |k\rangle = \text{Tr}\left(\rho_k \, P_\pm\right). \tag{A15}$$

Substituting (A13) and (A14) and using the Pauli algebra,

$$\text{Tr}(\mathbb{1}) = 2, \qquad \text{Tr}(\sigma_i) = 0, \qquad \sigma_i\sigma_j = \delta_{ij}\,\mathbb{1} + i\epsilon_{ijk}\sigma_k, \tag{A16}$$

50

one finds

$$A_{\pm}^{(k)} = \text{Tr}\left[\frac{1}{2}(\mathbb{1} + \vec{s}_k \cdot \vec{\sigma})\frac{1}{2}(\mathbb{1} \pm \hat{n} \cdot \vec{\sigma})\right]$$

$$= \frac{1}{4}\text{Tr}[\mathbb{1} \pm \hat{n} \cdot \vec{\sigma} + \vec{s}_k \cdot \vec{\sigma} \pm (\vec{s}_k \cdot \vec{\sigma})(\hat{n} \cdot \vec{\sigma})]$$

$$= \frac{1}{4}\left[2 \pm 2\,\vec{s}_k \cdot \hat{n}\right] = \frac{1}{2}\left(1 \pm \vec{s}_k \cdot \hat{n}\right). \tag{A17}$$

Using the definition (A2), this can be written equivalently as

$$A_{\pm}^{(k)}(w_1, w_2) = \frac{1}{2}\left[1 \pm \frac{\vec{s}_k \cdot \vec{\alpha}(w_1, w_2)}{|\vec{\alpha}(w_1, w_2)|}\right]. \tag{A18}$$

If $\gamma_k(w_1, w_2)$ denotes the angle between the Bloch vector $\vec{s}_k$ and $\vec{\alpha}(w_1, w_2)$, i.e.

$$\cos\gamma_k = \frac{\vec{s}_k \cdot \vec{\alpha}(w_1, w_2)}{|\vec{\alpha}(w_1, w_2)|}, \tag{A19}$$

then Eq. (A18) becomes

$$A_+^{(k)} = \frac{1}{2}\left(1 + \cos\gamma_k\right) = \cos^2\frac{\gamma_k}{2}, \qquad A_-^{(k)} = \frac{1}{2}\left(1 - \cos\gamma_k\right) = \sin^2\frac{\gamma_k}{2}, \tag{A20}$$

which makes explicit that $A_{\pm}^{(k)}$ are the probabilities to find the channel k aligned or antialigned with the geometric direction selected by the holonomy. In particular, all hadronic channels k share the same geometric eigenmodes $\Xi_{\pm}(w_1, w_2)$ and differ only in their projection coefficients $A_{\pm}^{(k)}$, thereby inducing nontrivial correlations among the corresponding physical form factors.

[1] V. Chung, *Infrared Divergence in Quantum Electrodynamics, Phys. Rev.* **140** (1965) B1110.

[2] P.P. Kulish and L.D. Faddeev, *Asymptotic conditions and infrared divergences in quantum electrodynamics, Theor. Math. Phys.* **4** (1970) 745.

[3] T.W.B. Kibble, *Coherent Soft-Photon States and Infrared Divergences. I. Classical Currents, J. Math. Phys.* **9** (1968) 315.

[4] T.W.B. Kibble, *Coherent soft-photon states and infrared divergences. ii. mass-shell singularities of green's functions, Phys. Rev.* **173** (1968) 1527.

[5] T.W.B. Kibble, *Coherent soft-photon states and infrared divergences. iii. asymptotic states and reduction formulas, Phys. Rev.* **174** (1968) 1882.

[6] T.W.B. Kibble, *Coherent soft-photon states and infrared divergences. iv. the scattering operator, Phys. Rev.* **175** (1968) 1624.

[7] A.P. Balachandran and V.P. Nair, *Dressing symmetry and gauge invariance, Phys. Rev. D* **98** (2018) 065007.

[8] J. Gamboa and F. Mendez, *QED-IR as topological quantum theory of dressed states, JHEP* **11** (2025) 040 [2507.11668].

[9] J. Gamboa, *Topological Structure of Infrared QCD*, 2511.07455.

[10] N. Brambilla, A. Mohapatra and A. Vairo, *Unravelling Pentaquarks with Born-Oppenheimer effective theory*, 2508.13050.

[11] R. Bruschini, *Heavy-quark spin symmetry breaking in the Born-Oppenheimer approximation, JHEP* **08** (2023) 219 [2303.17533].

[12] K.J. Juge, J. Kuti and C.J. Morningstar, *Gluon excitations of the static quark potential and the hybrid quarkonium spectrum, Nucl. Phys. B Proc. Suppl.* **63** (1998) 326 [hep-lat/9709131].

[13] K.J. Juge, J. Kuti and C.J. Morningstar, *Ab initio study of hybrid anti-b g b mesons, Phys. Rev. Lett.* **82** (1999) 4400 [hep-ph/9902336].

[14] B. Kang, X. Xia and T. Guo, *Hidden heavy flavor tetraquarks in the Born-Oppenheimer approximation, Phys. Rev. D* **111** (2025) 114016 [2503.10173].

[15] M. Berwein, N. Brambilla, A. Mohapatra and A. Vairo, *Hybrids, tetraquarks, pentaquarks, doubly heavy baryons, and quarkonia in Born-Oppenheimer effective theory, Phys. Rev. D* **110** (2024) 094040 [2408.04719].

[16] N. Isgur and M.B. Wise, *Weak Decays of Heavy Mesons in the Static Quark Approximation, Phys. Lett. B* **232** (1989) 113.

[17] N. Isgur and M.B. Wise, *Weak transition form factors between heavy mesons, Phys. Lett. B* **237** (1990) 527.

[18] H. Georgi, *An Effective Field Theory for Heavy Quarks at Low-energies, Phys. Lett. B* **240** (1990) 447.

[19] E. Eichten and B.R. Hill, *An Effective Field Theory for the Calculation of Matrix Elements Involving Heavy Quarks, Phys. Lett. B* **234** (1990) 511.

[20] B. Grinstein, *The Static Quark Effective Theory, Nucl. Phys. B* **339** (1990) 253.

[21] A.V. Manohar and M.B. Wise, *Heavy quark physics*, vol. 10 (2000), 10.1017/9781009402125.

[22] A.V. Manohar, *Introduction to Effective Field Theories*, 1804.05863.

[23] M. Neubert, *Heavy-quark symmetry, Phys. Rep.* **245** (1994) 259.

[24] A. Falk and M. Neubert, *Second order power corrections in the heavy quark effective theory*, *Phys. Rev. D* **47** (1992) 2965.

[25] N. Isgur and M.B. Wise, *Influence of the b* Resonance on anti-B —> pi e anti-electron-neutrino*, *Phys. Rev. D* **41** (1990) 151.

[26] CLEO collaboration, *Precise Determination of $|V_{cb}|$ from $\bar{B} \to D^*\ell^-\bar{\nu}$*, *Phys. Rev. Lett.* **82** (1999) 3746.

[27] BELLE collaboration, *Measurement of the CKM matrix element $|V_{cb}|$ from $B^0 \to D^{*-}\ell^+\nu_\ell$ at Belle*, *Phys. Rev. D* **100** (2019) 052007 [`1809.03290`].

[28] B.-I. Collaboration, *First semileptonic measurements in Belle II*, *Phys. Rev. Lett.* **127** (2021) 181802.

[29] BABAR collaboration, *Extraction of form factors from $\bar{B} \to D^{(*)}\ell\bar{\nu}$*, *Phys. Rev. D* **88** (2013) 052004.

[30] L. Collaboration, *Observation of excited D mesons in semileptonic B decays*, *JHEP* **2023** (2023) 144.

[31] J. Gamboa, *Topology and the infrared structure of quantum electrodynamics*, *JHEP* **07** (2025) 184 [`2505.13247`].

[32] E.J. Eichten and C. Quigg, *Quarkonium wave functions at the origin*, *Phys. Rev. D* **52** (1995) 1726 [`hep-ph/9503356`].

[33] M.E. Peskin and T. Takeuchi, *A New constraint on a strongly interacting Higgs sector*, *Phys. Rev. Lett.* **65** (1990) 964.

[34] M.E. Peskin and T. Takeuchi, *Estimation of oblique electroweak corrections*, *Phys. Rev. D* **46** (1992) 381.

[35] A.P. Szczepaniak and E.S. Swanson, *Coulomb gauge QCD, confinement, and the constituent representation*, *Phys. Rev. D* **65** (2001) 025012 [`hep-ph/0107078`].

[36] BABAR collaboration, *Measurement of the branching fractions and form-factor shapes of exclusive semileptonic B decays to D and D^**, *Phys. Rev. D* **79** (2009) 012002.

[37] B.I. Collaboration, *First Measurement of $\bar{B} \to D^*\ell\bar{\nu}$ with Belle II*, *Phys. Rev. Lett.* **127** (2021) 211801.

[38] RBC AND UKQCD collaboration, *$B \to D^*\ell\nu$ at zero recoil from 2+1-flavor lattice QCD*, *Phys. Rev. D* **103** (2021) 014510 [`2008.04140`].

[39] JLQCD collaboration, *B → D*ℓν form factors at nonzero recoil with 2+1-flavor QCD, arXiv preprint* (2023) [`2303.09449`].

[40] FERMILAB LATTICE AND MILC collaboration, *B → Dℓν form factors at nonzero recoil and $|V_{cb}|$ from 2 + 1-flavor lattice QCD, Phys. Rev. D* **92** (2015) 034506 [`1503.07237`].

[41] FLAG WORKING GROUP collaboration, *Flag review 2021, Eur. Phys. J. C* **82** (2022) 869.

[42] LHCB collaboration, *Measurement of the shape of the differential decay rate and the associated Isgur–Wise function for the decay $\Lambda_b^0 → \Lambda_c^+ \mu^- \bar{\nu}$, Phys. Rev. D* **96** (2017) 112005 [`1709.01920`].

[43] CLEO collaboration, *New CLEO Results for $|V_{cb}|$ and $|V_{ub}|$, arXiv preprint* (2002) [`hep-ex/0202029`].

[44] I. Caprini, L. Lellouch and M. Neubert, *Dispersive bounds on the shape of anti-B —> D(*) lepton anti-neutrino form-factors, Nucl. Phys. B* **530** (1998) 153 [`hep-ph/9712417`].

[45] CLEO collaboration, *Determination of the $\bar{B} \longrightarrow D^* \ell \bar{\nu}$ decay width and $|V(cb)|$, Phys. Rev. D* **67** (2003) 032001 [`hep-ex/0210040`].

[46] B. Collaboration, *Study of $B → D^{**} \ell \nu$ decays, Phys. Rev. D* **69** (2004) 112002.

[47] B.-I. Collaboration, *Updated results on $B → D^{**} \ell \nu$, Phys. Rev. D* **108** (2023) 012005.

[48] L. Collaboration, *Amplitude analysis of $B → D^{**} h$ decays, Phys. Rev. D* **101** (2020) 112007.

[49] J.D. Bjorken, *New symmetry relations in heavy flavor decays, SLAC-PUB-5278* (1990) .

[50] N. Uraltsev, *New exact heavy quark sum rules, Phys. Lett. B* **501** (2001) 86.

[51] M. Neubert, *Heavy quark symmetry, Phys. Rept.* **245** (1994) 259 [`hep-ph/9306320`].

[52] A.K. Leibovich, Z. Ligeti, I.W. Stewart and M.B. Wise, *Model independent predictions for $B → D_1(2420)\ell\bar{\nu}$ and $B → D_2^*(2460)\ell\bar{\nu}$, Phys. Rev. D* **57** (1998) 308 [`hep-ph/9705467`].

[53] BELLE collaboration, *Study of $B → D^{**} \ell \nu$ with a full angular analysis, Phys. Rev. D* **69** (2004) 112002 [`hep-ex/0307021`].

[54] BABAR collaboration, *Measurement of branching fractions of semileptonic B decays into narrow excited D mesons, Phys. Rev. Lett.* **101** (2008) 261802.

[55] F. Wilczek and A. Zee, *Appearance of gauge structure in simple dynamical systems, Phys. Rev. Lett.* **52** (1984) 2111.

[56] B. Simon, *Holonomy, the quantum adiabatic theorem, and berry's phase, Phys. Rev. Lett.* **51** (1983) 2167.

[57] M.V. Berry, *Quantal phase factors accompanying adiabatic changes*, *Proc. Roy. Soc. Lond. A* **392** (1984) 45.

[58] M. Nakahara, *Geometry, Topology and Physics*, CRC Press, 2nd ed. (2003).

[59] D. Tong, "Lectures on gauge theory and berry phases."
`http://www.damtp.cam.ac.uk/user/tong/`, 2005.

[60] M. Stone, *Berry phases in quantum field theory*, *Annals Phys.* **155** (1984) 56.

[61] A. Falk and M. Luke, *Strong decays of excited heavy mesons in chiral perturbation theory*, *Phys. Lett. B* **292** (1992) 119.

[62] J. Soto and S. Tomàs Valls, *Double-heavy Hadrons in the Born–Oppenheimer Approximation and Beyond*, *Acta Phys. Polon. Supp.* **17** (2024) 6.

[63] K.G. Wilson, *Confinement of Quarks*, *Phys. Rev. D* **10** (1974) 2445.

[64] C.G. Boyd, B. Grinstein and R.F. Lebed, *Constraints on form-factors for exclusive semileptonic heavy to light meson decays*, *Phys. Rev. Lett.* **74** (1995) 4603 [`hep-ph/9412324`].

[65] N. Isgur and M. Wise, *Weak decays of heavy mesons in the static quark approximation*, *Phys. Lett. B* **232** (1989) 113.

[66] A. Le Yaouanc, L. Oliver and J. Wagner, *Strong decays of D^{**} states*, *Phys. Rev. D* **56** (1997) 5668.

[67] B. Collaboration, *Measurements of semileptonic B decays to D^{**}*, *Phys. Rev. D* **82** (2010) 111101.

[68] F.e.a. Bernlochner, *Precision determination of $|V_{cb}|$ from $B \to D(*)\ell\nu$*, *Phys. Rev. D* **95** (2017) 115008.

[69] F.e.a. Bernlochner, *Global analysis including D^{**} states*, *Phys. Rev. D* **106** (2022) 053007.

[70] P. Gambino et al., *Inclusive and exclusive determinations of $|v_{cb}|$*, *Rev. Mod. Phys.* **92** (2020) 045003.

[71] M. Lavelle and D. McMullan, *Constituent quarks from QCD*, *Phys. Rep.* **279** (1997) 1.

[72] S. Fajfer, J.F. Kamenik and I. Nišandžić, *$B \to D^{(*)}\tau\bar{\nu}_\tau$ and the role of excited charm states*, *Phys. Rev. D* **85** (2012) 094025 [`1203.2654`].

[73] F.U. Bernlochner, Z. Ligeti, M. Papucci and D.J. Robinson, *Combined analysis of semileptonic B decays to D and D^*: $R(D^{(*)})$, new physics and $b \to c\tau\nu$*, *Phys. Rev. D* **95** (2017) 115008 [`1703.05330`].